ISPRS Journal of Photogrammetry and Remote Sensing 161 (2020) 246–262

Contents lists available at ScienceDirect

ISPRS Journal of Photogrammetry and Remote Sensing

journal homepage: www.elsevier.com/locate/isprsjprs

Accurate derivation of stem curve and volume using backpack mobile laser scanning

Eric Hyyppä[a,*], Antero Kukko[a,c], Risto Kaijaluoto[a], Joanne C. White[b], Michael A. Wulder[b], Jiri Pyörälä[a], Xinlian Liang[a], Xiaowei Yu[a], Yunsheng Wang[a], Harri Kaartinen[a,d], Juho-Pekka Virtanen[a,c], Juha Hyyppä[a,c]

[a] Department of Remote Sensing and Photogrammetry, Finnish Geospatial Research Institute, 02431 Masala, Finland
[b] Canadian Forest Service (Pacific Forestry Centre), Natural Resources Canada, 506 West Burnside Road, Victoria, British Columbia V8Z 1M5, Canada
[c] Department of Built Environment, Aalto University, 02150 Espoo, Finland
[d] Department of Geography and Geology, University of Turku, 20014 Turku, Finland

ARTICLE INFO

Keywords:
Mobile laser scanning
Stem curve
Stem volume
Tree volume
Mobile
SLAM

ABSTRACT

Forest inventories rely on field plots, the measurement of which is costly and time consuming by manual means. Thus, there is a need to automate plot-level field data collection. Mobile laser scanning has yet to be demonstrated for deriving stem curve and volume from standing trees with sufficient accuracy for supporting forest inventory needs. We tested a new approach based on pulse-based backpack mobile laser scanner (Riegl VUX-1HA) combined with in-house developed SLAM (Simultaneous Localization and Mapping), and a novel post-processing algorithm chain that allows one to extract stem curves from scan-line arcs corresponding to individual standing trees. The post-processing step included, among others, an algorithm for scan-line arc extraction, a stem inclination angle correction and an arc matching algorithm correcting for the drifts that are still present in the stem points after applying the SLAM algorithm. By using the stem curves defined by the detected arcs and tree heights provided by the pulse-based scanner, stem volume estimates for standing trees in easy (n = 40) and medium (n = 37) difficult boreal forest were calculated. In the easy and medium plots, 100% of pine and birch stems were correctly detected. The total RMSE of the extracted stem curves was 1.2 cm (5.1%) and 1.7 cm (6.7%) for the easy and medium plots, respectively. The RMSE were 1.8 m (8.7%) and 1.1 m (4.9%) for the estimated tree heights, and 9.7% and 10.9% for the stem volumes for the easy and medium plots, correspondingly. Thus, our processing chain provided stem volume estimates with a better accuracy than previous methods based on mobile laser scanning data. Importantly, the accuracy of stem volume estimation was comparable to that provided by terrestrial laser scanning approaches in similar forest conditions. To further demonstrate the performance of the proposed method, we compared our results against stem volumes calculated using the standard Finnish allometric volume model, and found that our method provided more accurate volume estimates for the two test sites. The findings are important steps towards future individual-tree-based airborne laser scanning inventories which currently lack cost-efficient and accurate field reference data collection techniques. The tree geometry defined by the stem curve is also an important input parameter for deriving quality-related information from trees. Forest management decision making will benefit from improvements to the efficiency and quality of individual tree reference information.

1. Introduction

Forests have a central role in a modern sustainable bioeconomy. Forests provide economical, ecological and social ecosystem services, such as timber, biofuel, habitat for biodiversity, recreation, functional food (berries and mushrooms) and climate regulation, to name a few examples (Kettunen et al., 2012). Inaccurate forest resource and biodiversity data can result in incorrect management decisions, which may

* Corresponding author at: Department of Remote Sensing and Photogrammetry, Finnish Geospatial Research Institute, 02431 Masala, Finland.
E-mail addresses: eric.hyyppa@gmail.com (E. Hyyppä), antero.kukko@nls.fi (A. Kukko), risto.kaijaluoto@gmail.com (R. Kaijaluoto), joanne.white@canada.ca (J.C. White), mike.wulder@canada.ca (M.A. Wulder), jiri.pyorala@helsinki.fi (J. Pyörälä), xinlian.liang@nls.fi (X. Liang), xiaowei.yu@nls.fi (X. Yu), yunsheng.wang@nls.fi (Y. Wang), harri.kaartinen@nls.fi (H. Kaartinen), juho-pekka.virtanen@aalto.fi (J.-P. Virtanen), juha.coelasr@gmail.com (J. Hyyppä).

https://doi.org/10.1016/j.isprsjprs.2020.01.018
Received 24 November 2019; Received in revised form 11 January 2020; Accepted 13 January 2020
Available online 31 January 2020

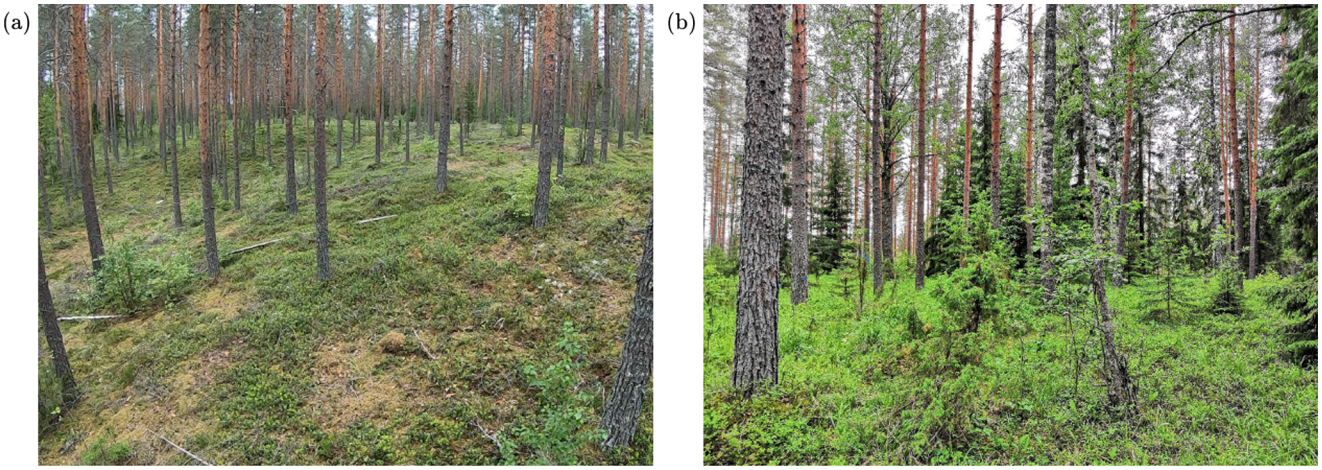

Fig. 1. Photographs of (a) the easy plot and (b) the medium plot.

have large economic and social impacts (Haara et al., 2019). Stem volume is among the most important tree attributes to be obtained in a forest inventory, and correlates strongly with tree biomass, the total volume of a tree, and many other ecological traits (Zianis et al., 2005). However, it is not possible or practical to measure the volume and other attributes of every single tree in a plot with conventional field measurement approaches, since individual tree measurement is costly and labour intensive.

Developments in laser scanning technologies (e.g., Lovell et al., 2003) have resulted in breakthroughs in the forest resource inventories. It has been estimated that Airborne Laser Scanning (ALS) -based inventories carried out every five years could provide added value to the decision-making at the level of 56e/ha (Kangas et al., 2019). Thus, improvements in the accuracy of forest inventories could greatly benefit both forest owners and all other parties involved in the wood trade. According to Kangas et al. (2019), the profit of forest owners could be increased by 4e/ha if the root-mean squared error (RMSE) of the stem volume estimates could be reduced by one percentage point. For the entire Finland, which currently has an estimated 20 Mha of economically-exploited forest, this would correspond to national savings in the order of 80 M€ with such an improvement in accuracy.

However, the calibration of ALS-based inventories (ALS prodiving the coverage of all forests to be measured) requires accurate field reference data at the individual tree and/or sample plot levels. The most commonly measured field reference data includes tree attribute information of tree species, stem diameter at breast height (DBH) or stem curve, and tree height. Throughout this paper, we use the term stem curve to refer to the stem diameter at different heights. Conventional measurements are conducted using calipers, measuring tapes and hypsometers. Stem volume is typically estimated using an allometric model based on the measured DBH, the tree height and possibly also the diameter at the height of 6 m. In a conventional area based inventory, some 300–600 field reference plots are needed for model calibration in Finland. These inventories would benefit from more automated and cost effective approaches to acquiring the required field reference data.

In recent years, several promising laser scanning techniques have been studied with the goal to automate plot-level field data collection. These methods encompass Terrestrial Laser Scanning (TLS) and Mobile Laser Scanning (MLS). The capacity and performance of state-of-art TLS and MLS, including UAV (Unmanned Aircraft Vehicle)-based measurements, to serve as field reference data for forest inventory in boreal forest conditions are summarized in Liang et al. (2019).

The TLS methods can be divided into two categories based on the number of scanning locations used within a single sample plot. In the single-scan TLS approach, the laser scanner is placed at the centre of the plot, and one panoramic full field-of-view scan is made. In the multi-scan TLS method, several scans are made to map the sample plot. Collecting the field data takes less time with the single-scan method in comparison to the multi-scan method; however, the single-scan method suffers from the omission of trees due to laser beam occlusion. In order to capture all trees in the plot, the multi-scan method is needed. Mature and robust algorithms applied to multi-scan TLS data provide high quality stem volume and biomass estimates that are comparable in accuracy with the best national allometric models (Liang et al., 2014a; Liang et al., 2018a).

Current shortcomings of the TLS methods include the aforementioned tree occlusion and need for multiple scans, as well as the lack of available software for processing and limited capacity to provide tree height information. Recently, Liang et al. (2019) proposed that the problem of obtaining accurate tree height estimates from TLS data could be resolved by combining TLS and UAV laser scanning data. This would allow the estimation of stem volume with a relative RMSE of 10% in boreal conditions, thereby enabling the use of stem volumes extracted from the TLS data as field reference data.

MLS techniques can be divided into phone-based scanning, vehicle-based scanning, Unmanned Aircraft Vehicle (UAV)- based, hand-held and other personal laser scanning techniques, including the backpack mobile laser scanning. It should be noted that MLS systems applied inside the forest canopy benefit greatly should they use SLAM (Simultaneous Localization and Mapping) technology, which enables accurate positioning of the scanner in forest environment hampering the GNSS (Global Navigation Satellite System) signal. SLAM technology has been incorporated into some commercial scanners, such as Gexcel HERON, Kaarta Stencil and GeoSLAM Horizon and Zebedee systems. Several experimental MLS systems incorporating SLAM have also been developed by different groups (e.g. Forsman et al., 2016; Kukko et al., 2017; Pierzchała et al., 2018). Past studies using MLS data have focused primarily on determining the DBH and the detection rate of trees (see, e.g., Chen et al., 2019; Cabo et al., 2018; Bauwens et al., 2016; Del Perugia et al., 2019; Marselis et al., 2016; Bienert et al., 2018; Čerňava et al., 2019; Zhao et al., 2018; Wu et al., 2013; Liang et al., 2014b, 2018b, 2019; Pierzchała et al., 2018; Saarela et al., 2017; Kukko et al., 2017). In the past studies, DBH has been obtained with accuracies ranging from 1 to 4 cm, and the detection rate for individual stems has varied between 80 and 95% in relatively easy forests (i.e. homogeneous relative sparse stands similar to that shown in Fig. 1(a)). Notably fewer studies reported the stem volume. The reported relative RMSE for stem volume ranges from 20 to 50% in easy and medium difficult boreal forest plots (Liang et al., 2018b, 2019; Bienert et al., 2018).

The objective of this study is to introduce a method for stem curve and volume estimation using mobile backpack laser scanning data that is sufficiently accurate to satisfy the operational requirements for field

inventory reference data collection. We demonstrate the method for individual trees (pines and deciduous trees) in boreal forest conditions. Our method is based on (1) a pulse-based 2D laser scanner (tilted from the vertical) mounted on a backpack and supplying dense point clouds and providing also tree heights with reasonable accuracy, (2) SLAM correction that allows us to reduce the positioning error of the MLS scanner inside the forest, (3) constructing the stem curve by matching good quality arcs obtained from different scan directions with a novel algorithm correcting for the positional drift that is still present in the stem points after the SLAM algorithm, (4) estimating the stem volume from the extracted stem curve without any allometric models as opposed to the conventional approach. Since both the stem curve and the tree height can be obtained from a single sensor, the stem volume can be estimated in a reliable manner. Herein, we compared the individual stem volumes obtained with the proposed MLS method against highly accurate field reference acquired semi-manually with multi-scan TLS. Additionally, the obtained volumes are compared against conventional volume measurements that are based on measuring the DBH with a caliper, the tree height with a hypsometer and subsequently estimating the stem volume using the national allometric stem volume model.

2. Materials and methods

2.1. Test sites

The two test sites used in this study were located in the boreal forest zone near Evo, Finland (61.19°N, 25.11°E). Each of the test sites had a size of 32 m × 32 m, and the main tree species on the sites were Scots pine (*Pinus sylvestris*), Norway spruce (*Picea abies*), Silver birch (*Betula pendula*), and Downy birch (*Betula pubescens*). These test sites were established in 2014 for the European Spatial Data Research (EuroSDR) Project of International Benchmarking of TLS in Forest inventory. In earlier studies (see, e.g., Liang et al., 2018, 2019, Wang et al., 2019a, 2019b), these forest stands were divided into three complexity categories ("easy", "medium", and "difficult") based on stem density, species composition of the vegetation, visibility of the tree stems, and the distribution of DBH values. Based on this classification, one of the test sites used in this study falls into the category "easy", whereas the other test site was classified as a "medium" plot. The test sites are shown in photographs in Fig. 1a and b.

The easy plot contains 42 trees corresponding to a stem density of 410 stems/ha, whereas the medium plot contains 44 trees corresponding to a density of 430 stems/ha. Although the stem densities on the plots are very similar, the other properties of the test sites differ markedly. As can be seen from Fig. 1a, the easy plot represents a typical managed forest in the boreal region of Finland with minimal understory vegetation and clear visibility. The trees in the easy plot are relatively homogeneous with small variations in the tree diameters and heights. Additionally, over 90% of the trees are pines, whereas the rest of the trees are spruces.

In the medium plot, the amount of understory vegetation is moderate, and the local stem density varies markedly within the plot. In the medium plot, there are also several spruces that are located within a short distance from other trees. Furthermore, the variations in the tree diameters and heights are notably larger than those of the easy plot, and the species composition is more varied. More detailed statistics of the plots are presented in Table 1.

2.2. Data acquisition with mobile laser scanning

The data for the study were collected using a kinematic Akhka-R3 backpack mobile laser scanning unit (see Fig. 2). The unit has been developed and built at the Finnish Geospatial Research Institute. The positioning system consists of a NovAtel Flexpak6 GNSS receiver and GGG-703 antenna to observe GPS and GLONASS satellites complemented with LITEF UIMU-LCI inertial measurement unit built on fiber optical gyroscopes and MEMS accelerometers to measure and output the movements of the platform at 200 Hz data rate. The 3D information of the forest is measured using a Riegl VUX-1HA laser scanner operating at 1550 nm wavelength and cross-track profiling of 360 degree field of view. This results in a dense helical scan pattern following the system trajectory to capture the ground and trees. The beam size is 4.5 mm at the exit, and diverges at a rate of 0.5 mrad resulting in a beam footprint of 6.6 mm at 10 m, and 13 mm at 25 m range. The ranging is specified to provide 5 mm accuracy with 3 mm precision (1σ) at 30 m range. At the maximum scan frequency, the scanner, using a revolving mirror, produces 250 cross-track profiles per second with 1017 kHz pulse repetition rate and can detect up to seven echoes per each pulse, which makes the instrument very attractive for vegetation analysis. Also, the reflectivity of the object surfaces are stored providing opportunities for spectral analysis, especially in foliage as the 1550 nm wavelength is sensitive to moisture - a possible early indicator for vegetation stress (Junttila et al., 2017).

Scans at the test sites were acquired using the maximum scan frequency of 250 Hz and 1017 kHz pulse rate. Thus, the angular step width for the study was 0.0885°, i.e. 0.00154 mrad, which corresponds to a 15.4 mm point spacing along the scan line at 10 m range. Along the track, the walking speed was typically 3–5 km/h resulting in a cross-track line spacing of 3–6 mm, respectively. The maximum unambiguous range at the given settings was 135 m for targets with 80% reflectivity. Darker surfaces, which natural forest surfaces, e.g. bark, leaves and needles typically are, yield shorter ranges: the specification for surfaces with 10% reflectivity is 50 m. However, the ranging is strongly dependent on the pulse repetition rate: with a lower frequency (user selectable 330, 507 and 762 kHz) a higher pulse energy and, thus, longer range can be achieved. Ranges beyond pulse rate specific unambiquity ranges can be solved in data processing using Riegl RiMTA software package provided that the signal is strong enough (sufficiently high surface reflectance) to get back to the scanner.

The 170 k€ worth system (with appropriate software) weighing about 15 kg could operate with swappable battery power for up to 8 h at a time. Single forest plot data collection could be done in minutes, but additionally the system initialization takes a few minutes at the beginning and at the end of data collection. Data georeferencing was carried out in RiWorld (Riegl Gmbh, Austria) supplemented with the trajectory processed in Waypoint Inertial Explorer (NovAtel Inc., Canada). Certain preparatory steps of the process were conducted in TerraScan (Terrasolid Ltd., Finland).

On the study sites, the data was collected by walking on the plot area to cover all the trees as completely as possible. The path was in

Table 1
Statistics of the forest stands on the two test sites. Note that only trees with their DBH exceeding 5 cm have been included in the statistics. The standard deviations of tree height and DBH are reported inside the parenthesis.

Test site	Number of trees	Stem density	Average DBH	Average tree height	Tree species distribution		
		(stems/ha)	(cm)	(m)	Pines (%)	Spruces (%)	Birches (%)
Easy	42	410	24.9 (±5.5)	20.6 (±3.0)	92.9	7.1	0.0
Medium	44	430	25.8 (±10.1)	20.5 (±6.2)	70.4	18.2	11.4

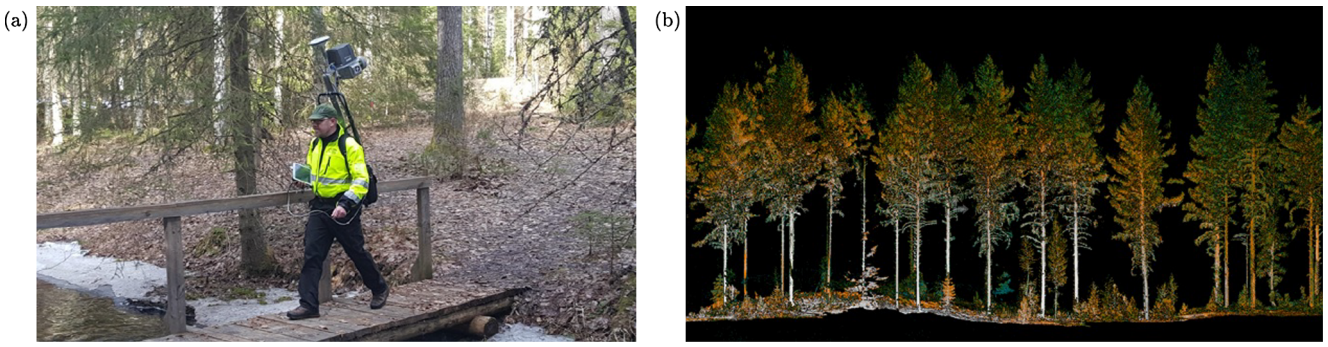

Fig. 2. (a) Akhka-R3 backpack mobile laser scanning system used in the study. Trajectory observations are recorded with a GNSS-IMU system while the laser scanner simultaneously measures the environment by cross track profiles 250 times a second. Data is stored on a tablet computer which also displays the on-the-fly trajectory data to aid the mapping in the forest. (Image: A. Kukko, 2016) (b) Cross section of the easy pine forest plot shows the potential of the backpack MLS technique in capturing the dominant tree stems and canopy structure, sub-dominant understory trees and terrain. Conducting the mapping from the ground helps the tree height determination and allows for DBH measurements.

general going around the plot to cover the trees from all four sides, and then the plot was split in four. Terrain and forest conditions, e.g. the saplings and bushes, fallen trees, big boulders, cliffs et cetera, regularly necessitate modifications to the routing on site. Ultimately, the scanning objective was to minimize the omission of trees, and in this study, the trajectories intersected multiple times within the plots to allow for loop closures providing key locations for trajectory optimization in the post-processing.

As the GNSS-IMU positioning is affected by the forest canopy, the trajectory solution deteriorates due to multipath effects and attenuation or complete loss of the GNSS signals. The post-processed differential solution (Waypoint Inertial Explorer) for the GNSS-IMU data collected by the Akhka-R3 positioning system for the trajectory is shown in previous studies to provide 0.5–0.8 m accuracy under boreal forest canopy (Kaartinen et al., 2015; Kukko et al., 2017), and the estimate holds for the data used in the study as well. This could be achieved using either physical or virtual GNSS base stations for the differential computation. However, such drifting of the trajectory solution can make it difficult to apply the MLS data for automated modeling without further geometric improvement.

2.3. Simultaneous localization and mapping

In a forest environment, trees block and degrade GNSS signals, which causes the trajectory solution of the scanning instrument to drift (e.g. Kaartinen et al., 2015). The drift can often be many meters even with high quality sensors. This drift can cause the acquired point clouds to have multiple copies of all objects since measurements taken at different time steps do not align spatially. To correct for this, we use a method inspired by SLAM methods, specifically the graph SLAM optimization method implemented and described in detail in Kukko et al. (2017). The steps of the method range from data collection, georeferencing, ground classification and other preparations for the raw point cloud data to trunk detection, trunk feature association, generating the graph representation of the features and the trajectory, optimization and finally georeferencing of the point cloud using the optimized trajectory.

In a traditional mobile robotics SLAM scenario, we often have an initial guess of the movement based on wheel odometry, which is then corrected with the help of sensors such as cameras or laser scanners. In our mobile laser scanner case, the initial guess of movement is the trajectory calculated from the GNSS and IMU measurements. While the GNSS/IMU trajectory drifts away from the real trajectory, the drift is gradual so we can extract features (in our case tree stems) that are measured over a short period of time from the point cloud based on the initial trajectory. As trees are static, the observations of them at different times, i.e., loop closures in terms of lidar/feature data reach, but not necessarily complete trajectory loops, enable us to correct much of the error found in the initial trajectory. This is done by formulating the initial trajectory as a pose graph and by minimizing the errors caused by the additional constraints gained from the observations of the tree stems. After optimization, the laser scanner measurements can be georeferenced again with the corrected trajectory in order to obtain a higher quality point cloud.

The pose graph optimization is commonly used in the robotics to perform simultaneous localization and mapping (SLAM) for mobile robots. For pose graph optimization the trajectory is formulated as a graph where the poses at consecutive timestamps (200 Hz in our case) and the detected features at certain time instance (captured as a mean of the feature points timestamps) form the nodes, and the edges (or constraints) between the nodes are formed from the measured relative transformations between them.

2.4. Reference measurements of stem curves, tree height and stem volume

In order to assess the performance of the proposed approach, we compared the estimated stem curves and stem volumes with values from high-quality reference measurements. The reference values for the stem curves were obtained with the help of a multi-scan TLS point cloud, from which the tree stems were manually detected and circles were manually fitted to the stem points at several different heights. The fitting aimed at overlapping the circle arc with the majority of stem points. The reference diameters were recorded at the heights of 0.65 m, 1.3 m, 2.0 m, 3.0 m and even upwards up to the maximum measurable height with one meter spacing. All trees with DBH over 5 cm were measured. The reference tree positions were determined based on the circle coordinates in the TLS point cloud at 1.3 m height when the tree was visible. Trees that were not visible in TLS point clouds were added to the tree map manually in the field using measuring tape and bearing compass.

Since the reference stem curves were based on TLS measurements conducted in 2014, the trees had roughly two years of time to grow between the reference measurements and the acquisition of the MLS data in April 2016. In order to estimate the tree growth between the years 2014 and 2016, we carried out field measurements of the DBH for all of the trees in the two test sites during the summer of 2019. Subsequently, we computed the increase in the DBH values between the years 2014 and 2019 for each of the trees separately, and interpolated the growth between the years 2014 and 2016 based on the measured 5-year growth. For each tree, it was assumed that the diameter had grown homogeneously on the whole height interval of the reference measurements. On average, the tree diameters had grown approximately 1.8 cm during the 5-year period, which corresponds to 0.7 cm growth between the years 2014 and 2016. Note that it is unlikely that the radial

growth increments have been the same at each height and at each year. However, this is the best assumption we can make without over-complicating the matter. The possible errors caused by this simplification were considered negligible when compared with other sources of errors due to measurements.

Reference heights for the trees were extracted from ALS data since it had been suggested and verified on these sample plots that ALS point clouds can yield very accurate tree height estimates (e.g., Liang et al., 2019; Wang et al., 2019a). For small trees shadowed by larger trees, the reference height was manually estimated as the height difference between the tree top and the digital terrain model created from the ALS point cloud. For large trees, the reference height was taken to be the difference between the digital terrain model and the average z coordinate of the five highest lying points within a range of 0.5 m from the tree location.

The reference values for stem volume were determined based on the reference measurements of stem curves and tree heights. Since there are no reference measurements for stem diameter close to the tree top, the stem curve has to be extrapolated in this height interval based on existing data. To achieve this, we fitted a parabola

$$R_1(z) = a_1(h - z)^2 + a_2(h - z), \tag{1}$$

and a square root function

$$R_2(z) = b_1\sqrt{h - z} \tag{2}$$

to the reference measurements of stem radii R at different heights z. In Eqs. (1) and (2), h is the reference height of the tree, and $\{a_1, a_2, b_1\}$ are parameters to be determined with ordinary least squares regression. Note that both of the fitting functions force the stem radius to equal zero at the top of the tree for all parameter values. After determining the fitting parameters, the reference stem volume V was determined as

$$V = \frac{\pi}{2}\left(\int_0^h R_1(z)^2 \mathrm{d}z + \int_0^h R_2(z)^2 \mathrm{d}z\right) = \pi \int_0^h R_{\mathrm{eff}}(z)^2 \mathrm{d}z, \tag{3}$$

i.e., the volume was taken to be the average value predicated by the fits. Note that $R_{\mathrm{eff}}(z) = \sqrt{R_1(z)^2 + R_2(z)^2}/2$ is the effective radius corresponding to the volume estimate. This fitting procedure is illustrated in Fig. 3, where we show one reference stem curve with the effective diameter $D_{\mathrm{eff}} = 2R_{\mathrm{eff}}$, and the fits based on Eqs. (1) and (2).

The fitting process used to estimate the reference volume has several advantages. First, the fitting functions can approximate the shape of a stem curve as shown in Fig. 3. Second, the risk of over-fitting is minimal due to the small number of fitting parameters. As a result of the gap between the highest measurable stem diameter and the tree top, the risk of over-fitting is substantial for more complicated models involving several parameters. For example, the model used by Laasasenaho (1982) is a polynomial of degree 34 and would therefore be prone to severe over-fitting.

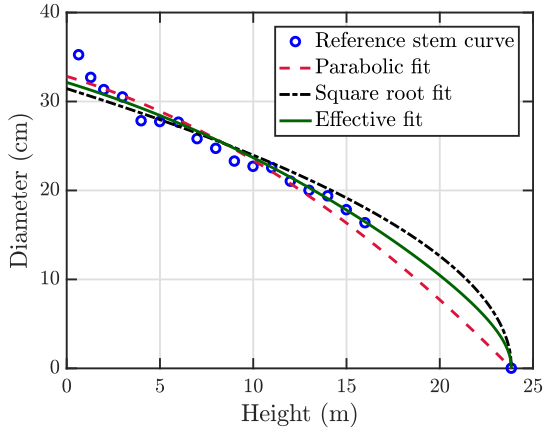

Fig. 3. In order to determine the reference volume, we fit a square root function (dotted black line) and a parabola (dashed red line) to the reference stem curve (blue circles). The stem volume is obtained as the average of the volumes estimated with the parabolic and square root fits. This corresponds to the effective fit shown with the solid green line.

To further estimate the accuracy of the reference volumes, we note that there are three possible sources contributing to the error: the reference diameter measurements, the reference height measurements and the fitting process itself. The accuracy of the manually measured stem diameter references from TLS point clouds have reportedly low RMSE (RMSE $<$ 1 cm). The overall effect of these errors to tree-specific stem volume estimations has varied between 1 and 10%, in conditions similar to those in this study (Saarinen et al., 2017).

By comparing the tree heights extracted from the ALS point cloud against ordinary field measurements, we have additionally estimated that the error in the reference heights should be at most 0.4 m (2%). Importantly, a small error in the tree height only affects the fit at heights above the highest reference diameter (see Fig. 3). This has allowed us to estimate that the error in the reference volumes due to the uncertainty in the reference heights is on the order of 1% in our case, where the reference diameters extend to the height of 13 m on average. Furthermore, we have estimated that the relative RMSE of stem volume due to the fitting process itself is on the order of 1–2% on the height interval, where reference diameter measurements are available. Since this height interval contains on average over 80% of the volume of the whole stem, it is probable that the error introduced by the fitting process is on the order of 2–3% for the volume of the whole stem.

2.5. Statistical analysis

Here, we briefly present the statistical methods used for evaluating the performance of the proposed algorithm. In order to quantify the accuracy of stem detection, we use the completeness and correctness defined as

$$\text{Completeness} = \frac{\text{Number of reference trees found}}{\text{Total number of reference trees}} \times 100\%, \tag{4}$$

$$\text{Correctness} = \frac{\text{Number of reference trees found}}{\text{Total number of trees found}} \times 100\%, \tag{5}$$

where the total number of trees found refers to the trees found within the 32 m × 32 m test site.

The bias and root-mean-square error (RMSE) of a variable x are computed as

$$\text{bias} = \sum_{i=1}^{N} \frac{x_i - x_{i,\mathrm{ref}}}{N}, \tag{6}$$

$$\text{RMSE} = \sqrt{\sum_{i=1}^{N} \frac{(x_i - x_{i,\mathrm{ref}})^2}{N}}, \tag{7}$$

where N is the number of matched trees, $\{x_i\}_{i=1}^N$ denotes the set of estimated values, and $\{x_{i,\mathrm{ref}}\}_{i=1}^N$ are the corresponding reference values. Additionally, we use the following definitions for the corresponding relative bias and RMSE

$$\text{bias} - \% = \frac{\text{bias}}{\bar{x}_{\mathrm{ref}}} \times 100\%, \tag{8}$$

$$\text{RMSE} - \% = \frac{\text{RMSE}}{\bar{x}_{\mathrm{ref}}} \times 100\%, \tag{9}$$

where $\bar{x}_{\mathrm{ref}}$ is the mean of the reference values.

Note that the bias and RMSE of stem curve estimates has to be computed in a slightly different way since we obtain a varying number of diameter estimates for each tree. Therefore, we compute the total bias and RMSE for the stem curve estimates as

$$\text{bias} = \frac{1}{N}\sum_{i=1}^{N}\sum_{j=1}^{N_i}\frac{D_i(z_j) - D_{i,\text{ref}}(z_j)}{N_i}, \tag{10}$$

$$\text{RMSE} = \sqrt{\frac{1}{N}\sum_{i=1}^{N}\sum_{j=1}^{N_i}\frac{(D_i(z_j) - D_{i,\text{ref}}(z_j))^2}{N_i}}, \tag{11}$$

where N_i is the number of successfully extracted diameter estimates for the ith tree, $D_i(z_j)$ is the extracted diameter of the ith tree based on the smoothing spline fit evaluated at the height z_j, and $D_{i,\text{ref}}(z_j)$ is the corresponding reference value. Note that we can compare the extracted diameters with the reference values only at such heights for which both of the values exist. Therefore, the number of heights used for comparison N_i depends on the height range that yields good quality arcs.

3. Theory of the proposed algorithm

In this section, we introduce the algorithm that allows for the extraction of the stem curve and volume from an MLS point cloud. The goal of the algorithm is to extract arcs of good quality from the scan lines cast on the tree trunks, and subsequently, cluster these arcs into groups corresponding to individual trees. In order to obtain an accurate stem curve estimate for each tree, we further match the arcs and correct for the possible inclination of the tree stem. It should be noted that the algorithm is fully automatic and does not require any manual processing of the data. We present the flow chart of the proposed algorithm in Fig. 4.

3.1. Digital terrain model and watershed segmentation

First, a DTM (Digital Terrain Model) is created from the point cloud in order to find out the ground elevation of the test sites. To generate the DTM, we apply a voxel-based method, in which the test site is divided into 50 × 50 pixels in the xy plane and further to 20 height intervals in the z direction. For each pixel, the ground level is assumed to lie in the lowest height interval containing sufficiently many points (> 1%) as compared with the total number of points within the pixel. Subsequently, the ground level in the pixel of interest is obtained by taking the average elevation of the points within this ground voxel. After applying Gaussian smoothing for the discretized ground elevation, we obtain the final DTM. To proceed, we subtract the ground elevation from each data point in the point cloud so that the new z coordinates represent point heights from the ground.

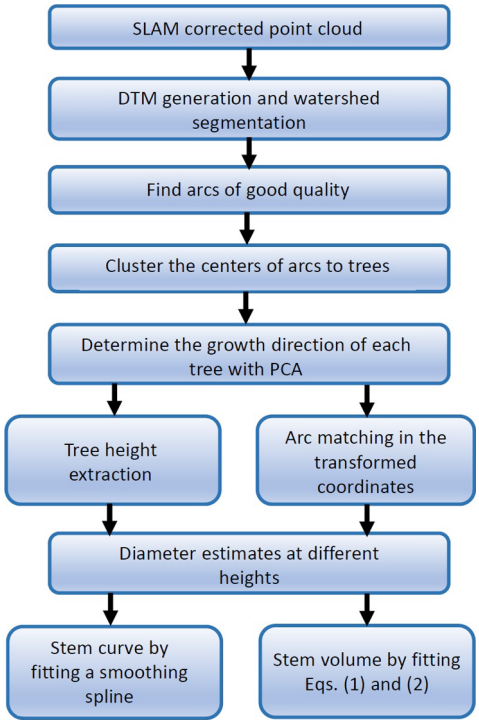

Fig. 4. Flowchart illustrating the proposed algorithm.

Subsequently, we perform segmentation for the point cloud in order to divide the sample plot into smaller regions that contain roughly one tree. This is advisable since dividing the data into smaller segments can greatly reduce the time needed to experiment with the parameters of the arc extraction algorithm (see Section 3.2). To perform the segmentation, we first form the canopy height model by finding the height of the highest point within each pixel (see, e.g., Hyyppä et al., 2001). After applying Gaussian smoothing to the canopy height model, we perform watershed segmentation in order to divide the test site into watershed regions (Hyyppä et al., 2001). Note that each watershed region can be treeless, or contain one or several trees. It is also possible that some trees end up partly in different watershed regions.

3.2. Arc finding and clustering individual arcs to trees

In the next stage of the algorithm, we aim to extract arcs of good quality from the points measured from the tree trunks. Fig. 5 illustrates a couple of arcs formed by consecutive points reflected from the same tree. The extraction of individual arcs has many advantages as compared with many other approaches used for stem detection. First, the positioning errors of the mobile laser scanner can be on the order of 10–20 cm even after applying the SLAM algorithm (as described in Section 2.3). According to previous studies, the positioning error of MLS without SLAM is in the order of 80 cm (Kaartinen et al., 2015). Despite the SLAM correction, the positioning error of the scanner can result in severe deformation of the stems in the point cloud. This deformation of the stems can easily propagate to errors in the diameter estimates if the detection of stem points is not based on arc finding or equivalent methods. Second, the points from tree branches can efficiently be filtered out by reconstructing the stem from individual arcs. The same does not apply for, e.g., methods, in which the tree stem is divided into height intervals in order to perform circle or cylinder fitting at different heights (Raumonen et al., 2013).

Our arc finding algorithm can be viewed as an extension of that proposed by Forsman et al. (2016). Since the data points recorded by the 2D laser scanner are in time order, we can find individual scan-line arcs by monitoring the distance between consecutive data points. The key idea of the algorithm is that a large distance between consecutive points indicates that the points have not been reflected from the same stem. Unlike Forsman et al. (2016), we aim to find arcs at all heights instead of just the breast height, and we do not always stop the arc due to a few noise points in the middle of an arc (e.g. in order to account for tree branches).

We also set specific quality criteria for the arcs, which allows us to only extract arcs of requested quality, as described in detail below. With the parameter values used in this study, the typical number of arcs for a single tree ranges from hundreds of arcs to thousands of arcs. Note that we use exactly the same parameter values for both of the test sites. More precisely, the algorithm with the quality criteria is summarized as follows:

1. Suppose P_i is the first point of the current arc candidate. On the first round, P_i is naturally the first point P_1 of the data set. Accumulate new points to the arc candidate until the distance between consecutive points exceeds a threshold value ($d_{\max}$ = 3 cm).
   a. If the current arc candidate contained less than N_{start} = 10 points before a large gap ($d_{\max}$ = 3 cm), we neglect the arc candidate and start accumulating a new arc candidate according to instruction 1 but using P_{i+1} as the new starting point.
   b. If the current arc candidate contained 10 points or more before the large gap, we fit a circle to the arc candidate after projecting

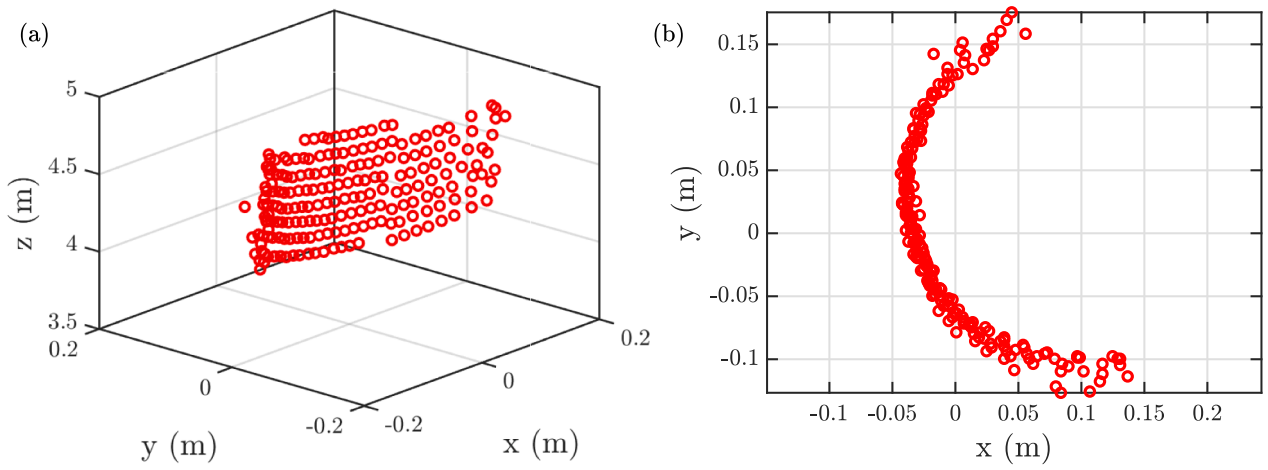

Fig. 5. (a) 3D view of a couple of good quality arcs corresponding to a tree trunk. Note that the scale of the z axis is not equal to that of the x and y axes. (b) 2D projection of the points shown in panel (a).

it on to the xy plane.

i. If one or more of the next $N_{\text{noise,max}} = 5$ points is located within $l_{\text{max}} = 8$ mm of the arc of the fitted circle in the xy plane, we continue accumulating the arc candidate from the first point within 8 mm of the fitted circle. When the next large gap is detected, we proceed based on the instruction 1(b). Note that the noise points far from the arc candidate are not included in the arc candidate.

ii. If none of the next 5 points is located within 8 mm of the fitted circle, we stop accumulating the arc. If the arc candidate contains over $N_{\text{min}} = 30$ points, we move to testing the quality of the arc as explained in instruction 2. After the possible quality testing, we start accumulating a new arc candidate according to instruction 1 but using the first of the previous 5 noise-type points as the starting point.

2. The arc candidate with over 30 points is tested for quality before it is accepted as a proper stem arc. We fit a circle to the arc candidate after projecting it on to the xy plane. The arc candidate is accepted as an arc if the radius of the fit is between $R_{\text{min}} = 3$ cm and $R_{\text{max}} = 40$ cm, the central angle of the arc is above $\theta_{\text{min}} = 0.6\pi\text{rad} = 108^{\circ}$, and the standard deviation of the radial residuals is below $\sigma_R = 6$ mm.

Note that the parameters of the arc finding algorithm are chosen based on the typical distance of consecutive points in the point cloud, the noise level of the arcs, the features of the forest and the desired accuracy of the extracted stem curve. The parameter values have been selected based on heuristics and physics of the point clouds as mentioned. Higher performance for tree attribute retrieval can be obtained by optimizing them more carefully.

It is a well-known problem that the finite width and footprint of the laser beam can result in a slight distortion of the arcs and thus an overestimation of the tree diameter (Forsman et al., 2018). As can be seen from Fig. 5b, this effect is typically most prominent close to the edges of an arc, and therefore, we drop two points from the beginning and ending of each arc following a strategy slightly modified from m Forsman et al. (2016). Furthermore, it should be noted that the arc finding algorithm is applied to points located over 1 m above the ground level since reflections from the ground and the understory vegetation can result in unreliable arcs.

For the circle fitting, we use the algebraic fit proposed by Al-Sharadqah and Chernov (2009) since it is efficient to compute and it is hyperaccurate in the sense, that it approximates the geometric least-squared-distance fit with no bias at all. Thus, the hyperaccurate fit is a clear improvement over the simple Kåsa fit (Kåsa, 1976) that tends to underestimate the radius for short and noisy arcs (see, e.g., Pratt, 1987; Al-Sharadqah and Chernov, 2009), and it is also a slight improvement over the Pratt fit (Pratt, 1987). It is noteworthy that in contrast to other approaches (e.g., Liang et al., 2012) we do not need to utilize robust but slow circle finding algorithms since the arc finding algorithm automatically filters out data points that correspond to reflections from the branches.

The hyperaccurate circle fit amounts to solving the following generalized eigenvalue problem

$$\mathbf{Z}^T\mathbf{Z}\beta = \lambda\mathbf{S}\beta, \tag{12}$$

where the ith row of $\mathbf{Z}$ equals $\mathbf{Z}_{i:} = (x_i^2 + y_i^2, x_i, y_i, 1)^T$, β is a coefficient vector $\beta = (A, B, C, D)^T$ corresponding to a circle $A(x^2 + y^2) + Bx + Cy + D = 0$, λ is the generalised eigenvalue and $\mathbf{S}$ is a matrix encoding the hyperaccurate circle constraint

$$\mathbf{S} = \begin{pmatrix} 8\bar{z} & 4\bar{x} & 4\bar{y} & 2 \\ 4\bar{x} & 1 & 0 & 0 \\ 4\bar{y} & 0 & 1 & 0 \\ 2 & 0 & 0 & 0 \end{pmatrix}, \tag{13}$$

where $\bar{z}$ denotes the mean value of the set $\{x_i^2 + y_i^2\}_{i=1}^N$, and $\bar{x}$ and $\bar{y}$ denote mean values of x and y coordinates, respectively. The coefficients β of the hyperaccurate circle fit are obtained as the generalized eigenvector minimizing the function $\|\mathbf{Z}\beta\|_2^2 = \beta^T\mathbf{Z}^T\mathbf{Z}\beta$. The center of the fitted circle (x_0, y_0) and the radius R can readily be solved from the coefficients as

$$x_0 = -\frac{B}{2A}, y_0 = -\frac{C}{2A}, R = \sqrt{\frac{B^2 + C^2}{4A^2} - \frac{D}{A}}. \tag{14}$$

After finding the arcs, the centers of the arcs are clustered in the xy plane by applying the DBSCAN algorithm (Ester et al., 1996) in order to determine which arc corresponds to which tree. By combining the arc finding algorithm with DBSCAN clustering, it is possible to reconstruct the stems without any points reflected from branches or understory vegetation. The parameters of the DBSCAN clustering are the neighborhood radius ε that gives the length scale for the smallest possible separation of two clusters and the point number threshold N_{minPts} that is used to determine whether a certain point is a core point within a cluster. A large range of DBSCAN parameter values result in an equally good clustering since the distance between different trees is markedly larger than the deviation of the arc centers corresponding to a single tree.

In our implementation, we set $N_{\text{minPts}} = 25$ and use 25 cm as the neighborhood radius ε since it can be safely assumed that the inter-tree distance is larger than the mean DBH≈ 25 cm. Note that our choice of N_{minPts} implies that a tree needs to yield at least 25 arcs for it to be

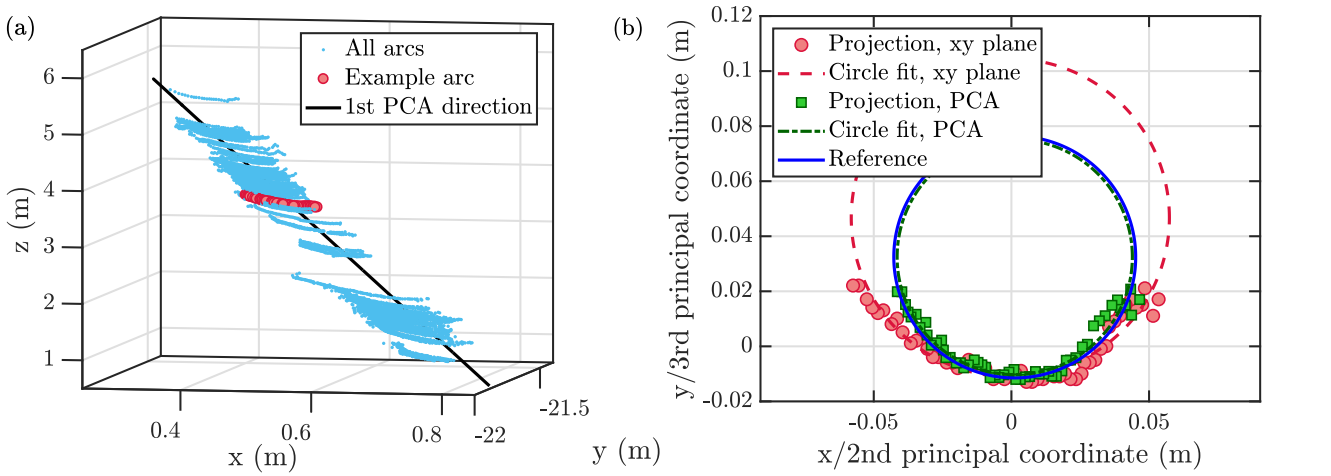

Fig. 6. (a) 3D view of all the extracted arcs (light blue dots) of a birch with inclination of $\theta = 8.6^{\circ}$ with respect to the vertical direction. The red circles illustrate the arc selected as an example, and the first principal direction is shown with a black line. Note that the scale of the z axis does not equal that of the x and y axes, which makes the tree look more inclined than it actually is. (b) Projection of the example arc to the xy plane (red circles) and to the plane perpendicular to the 1st principal direction (green squares). The dashed lines show the circular fits and the solid blue line illustrates a circle whose radius equals the reference value.

detected in the clustering. Note also that it is advantageous to find the arcs in each of the watershed regions separately and thus perform DBSCAN clustering only for a small number of trees at a time if a simple quadratic implementation of the DBSCAN algorithm is used. After the clustering, we check whether there are trees whose arcs have ended up in two neighboring watershed regions. This can be done by combining all pairs of trees that have an inter-tree distance on the order of their radii.

3.3. Correcting the effect of a non-zero inclination angle with principal component analysis

Due to the inclination of the mobile laser scanner with respect to the horizontal direction, the extracted arcs are not horizontal but clearly inclined. The highest and lowest point elevation within a single arc can differ by several tens of centimeters or even half a meter. Therefore, the inclination of a particular tree stem can result in major underestimation or overestimation of the stem diameter when the inclination angle of the tree exceeds: 3–4°. Fig. 6a shows an inclined tree in the medium plot, for which the stem diameters are clearly overestimated when the circle fitting is performed in the xy plane as illustrated in Fig. 6(b).

To correct for this error source, we note that the arcs should be projected to the plane perpendicular to the growth direction of the tree before the final circle fitting. The growth direction of a tree can be found by applying principal component analysis to the arc centers found for a tree. The growth direction is given by the first principal direction. This correction clearly improves the diameter estimates for the most inclined trees as can be seen from the example shown in Fig. 6(b).

3.4. Arc matching and stem curve extraction

In order to determine the stem curve of an individual tree, we divide the arcs into height intervals based on the average z coordinate of the arcs. In our implementation, the height intervals have a constant width of 20 cm and they start upward from 1 m above ground. To accurately estimate the stem diameter within each height interval, we use a procedure that aims to match the arcs optimally in order to avoid any errors resulting from the positioning errors of the mobile laser scanner (post-SLAM correction). The idea of matching displaced stem models corresponding to a single tree has previously been considered by Holmgren et al. (2019) and Čerňava et al. (2019). Holmgren et al. (2019) use tree spine calibration to refine the stem model first using multiple trees in the calibration and subsequently refining the stem model for each tree individually. The approach adopted by Čerňava et al. (2019), aims to match the extracted stem models of a single tree in three dimensions by first identifying the stem model with the highest number of points and then applying a translation to each of the other stem models such that they match as well as possible with the stem model with the highest number of points. However, this approach requires that there is sufficient overlap between the stem models to be matched, which is not always the case.

In this section, we present a different approach to this post-SLAM matching problem, which does not require any overlap between the arcs to be matched but assumes that the stem is approximately circular. Note that the goal of this arc matching algorithm is to improve the modeling accuracy of each of the detected stems and not to perform SLAM for the entire point cloud. Before matching the arcs belonging to a certain height interval, we project the points to the plane perpendicular to the growth direction of the tree as explained in the previous section. The arc matching algorithm can be summarized as follows:

1. First, we fit a circle with the hyperaccurate circle technique to each of the arcs separately. This is illustrated with three simulated arcs in Fig. 7(a). Based on the circle fits, we center the arcs such that the centers of the fits coincide with the origin after applying the translation.
2. Subsequently, we fit a single circle to all of the data points. Importantly, the center of the fitted circle is fixed to the origin. This is illustrated in Fig. 7(b).
3. Next, we separately fit to each of the arcs a circle with its radius being fixed to the value obtained in the previous step. Based on the centers of the fitted circles, all of the arcs are re-centered such that the new center coincides with the origin. This is illustrated in Fig. 7(c). The steps 2 and 3 are re-iterated for sufficiently many times until the algorithm converges. In our implementation, we use 5 iterations by default.
4. Finally, the radius of the matched arcs is estimated by fitting a circle to all of the data points. Again, the center of the fitted circle is fixed to the origin. The resulting fit for the simulated data is shown in Fig. 7(d).

Fitting a circle with its center fixed to the origin can be realized easily as follows

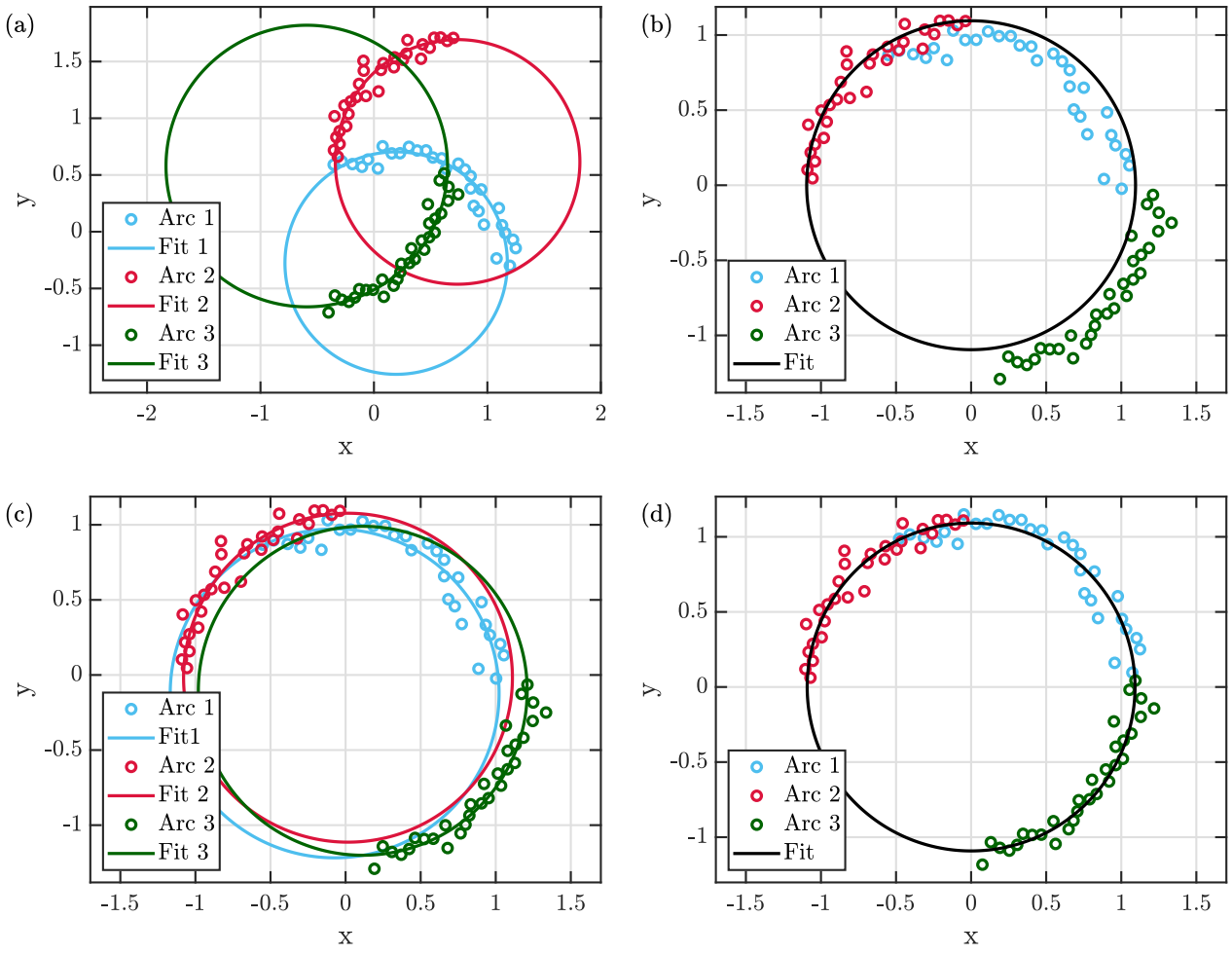

Fig. 7. Schematic of the arc matching algorithm. (a) Three simulated arcs of 30 points with normally distributed noise. The circles drawn with the solid line illustrate the hyperaccurate circle fit to each of the arcs. (b) The same arcs after shifting their coordinates such that the center of each fit coincides with the origin. The solid black line illustrates a circular fit with the center fixed at the origin. (c) Subsequently, we fit a circle to each of the arcs such that the radius of each fit is forced to equal the radius obtained in panel (b). (d) After iterating the process presented in panels (b) and (c), we obtain the final fit shown with the solid black line.

$$R_{\text{fit}} = \sum_{i=1}^{N} \frac{\sqrt{x_i^2 + y_i^2}}{N}, \tag{15}$$

where R_{fit} is the least-squared-distance fit of the radius, N is the number of data points and $\{(x_i, y_i)\}_{i=1}^{N}$ is the set of data points. However, fitting a circle with a fixed radius is not as straightforward, and to our knowledge, there does not exist any non-iterative methods for this constrained optimization problem. Therefore, we formulate the problem as a nonlinear optimization problem, where the objective function f to be minimized is the sum of squared radial residuals

$$f(x_0, y_0) = \sum_{i=1}^{N} (\sqrt{(x_i - x_0)^2 + (y_i - y_0)^2} - R_{\text{fixed}})^2, \tag{16}$$

where (x_0, y_0) is the circle center to be determined and R_{fixed} is the fixed value of the radius.

In Fig. 8(a) and (b), we illustrate the performance of the arc matching algorithm for arcs extracted from a pine located in the medium category plot. As can be seen from Fig. 8(b), the algorithm manages to match the displaced arcs well even though the arcs on different sides of the tree do not properly overlap. Note that it is possible but rare that the arcs to be matched are from different trees that are located nearby. In this case, the arc matching algorithm can produce an unreliable diameter estimate which can, however, be filtered out using the outlier removal step described below.

For each tree, the diameter is estimated with arc matching at all the height intervals containing at least 3 arcs. We model the stem curve with a cubic smoothing spline (see, e.g., De Boor, 1978; Pollock, 1993) fitted to the diameter estimates since a smoothing spline provides a non-parametric fit that has suitable smoothness properties for stem curve modeling (e.g., Nummi and Möttönen, 2004; Koskela et al., 2006; Saarinen et al., 2017). Before fitting the smoothing spline, we try to automatically remove clearly outlying diameter estimates. A diameter estimate D_j at height z_j is deemed as outlying using the following process:

1. Find the k nearest height intervals for the height z_j (including the height interval itself), and determine the median (MEDIAN) and median absolute deviation (MAD) for the diameter estimates corresponding to these k height intervals. The point (z_j, D_j) is deemed as outlying if both of the following conditions are satisfied
   (a) $|D_j - \text{MEDIAN}| > 2 \times \text{MAD}$
   (b) $|D_j - \text{MEDIAN}| > 3.0$ cm

Note that median is a robust estimator of location and median absolute deviation is a robust estimator of scatter and therefore, they are appropriate for detecting whether a data point is an outlier. In our implementation, we use $k = 5$.

When fitting the smoothing spline to the diameter estimates, we neglect the diameter estimates classified as outliers. In the fitting process, we also weight each diameter estimate by the inverse of the

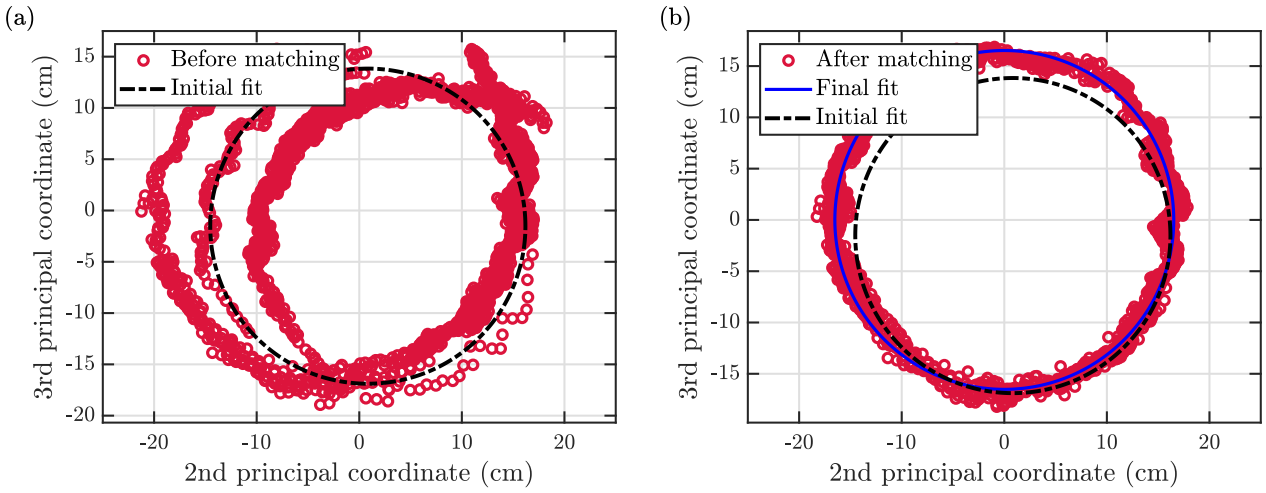

Fig. 8. (a) Arcs of a pine in the medium plot before applying the arc matching algorithm. The data points (red circles) correspond to arcs having a mean z coordinate in the range 1.2–1.4 m. The dashed black line illustrates the hyperaccurate circle fit to the data points. (b) The same arcs after applying the arc matching algorithm. The solid blue line illustrates the circular fit obtained as a result of the arc matching procedure. Note that in both figures, we have projected the data points to the plane defined by the 2nd and 3rd principal directions in order to correct the non-zero inclination of the tree.

uncertainty estimate of the diameter. The uncertainty estimate of the diameter is, thus, given by

$$\Delta D = \frac{2}{\sqrt{N}}\left(\sum_{i=1}^{N}\frac{(\sqrt{(x_i-x_0)^2+(y_i-y_0)^2}-R)^2}{N}\right)^{1/2}, \tag{17}$$

where N is the total number of points in all arcs within the height interval of interest, and the coordinates (x_i, y_i) refer to the coordinates after the arc matching. The optimal value for the smoothing parameter λ is chosen separately for each tree by applying leave-1-out cross validation. Some examples of the resulting stem curves are illustrated in Fig. 10 in Sec. 4.2 and in Figs. A14-A17 in the Appendix. As can be seen from the figures, clear outliers are rare even for quite difficult trees.

3.5. Tree height and stem volume

The advantage of MLS is in the capacity to measure both the stem curve and the tree height simultaneously leading to accurate stem volume estimation. Surprisingly it has not been applied earlier. As demonstrated by Bienert et al. (2018), it should be possible to determine the heights of individual trees with an accuracy on the order of 1 m from MLS data. Following the approach of Liang et al. (2018b), we determine the heights in a different way for large and small trees since small trees might be shadowed by larger trees. For all trees, we first find all points that are located within 0.5 m of the 3D line defined by the mean position of the tree and the growth direction of the tree. Subsequently, we divide the z axis to height intervals with a uniform spacing of 0.5 m, and count the number of points within each height interval for each tree separately. For large trees with the stem diameter exceeding 20 cm at some height, the tree height is obtained as the average of the 5 highest points in the highest height interval containing at least 10 points. This allows us to exclude outlying points located above the canopy. For small trees with the stem diameter below 20 cm at all heights, we first find the lowest height interval that is above the highest extracted arc and contains less than 20 points. It is assumed that this height interval is located right above the height interval containing the tree top. Subsequently, the tree height is set to equal the average z coordinate of the 5 highest points within the height interval corresponding to the tree top.

Having extracted the stem curve and the tree heights for all the extracted trees, the stem volume can be estimated by applying the fitting procedure explained above in Sec. 2.4. Note that we neglect the outlying diameter estimates also in the volume estimation.

4. Results

4.1. Tree detection

In order to compare the trees found using our algorithm with the reference trees, we matched each found tree with the closest reference tree provided that the distance between our detected tree and the reference tree was less than 0.5 m. For the easy plot, we detect 40 out of the 42 reference trees, i.e., the completeness of stem detection is 95%. The algorithm is able to detect all of the 39 pines meaning that the completeness of pine detection is 100%. However, the algorithm detected only 1 out of the 3 spruces, due to the large number of branches and the poor visibility of spruce stems.

In the medium plot, our algorithm found 37 out of the 44 reference trees, i.e., the completeness of stem detection was 84%. Again, the algorithm detected all of the 31 pines and also all of the 5 birches, but only one of the 8 spruces. The only spruce detected by our algorithm was the largest and oldest of the 8 spruces, and therefore, it does not have as many branches as the other spruces in the lower part of its stem as illustrated in Fig. A17. The spruces that were not detected are relatively small with a mean DBH of approximately 10 cm and the detection suffers from poor stem visibility due to the branch structure natural to them. The correctness of stem detection for pines and birches was again 100%.

4.2. Stem curve

In this section, we compare the stem curves extracted using our algorithm against the reference measurements. On average, our algorithm manages to extract arcs of good quality in the height interval of 1.2–7.4 m for the easy plot. The corresponding height range for the medium plot was 1.4–7.8 m. Depending on the properties of the tree, the height of the highest good quality arc ranges from approximately 4 m to 10 m.

Using the definitions of Sec. 2.5, the total RMSE of the extracted stem curves was 1.2 cm (5.1%) for the easy plot and 1.7 cm (6.7%) for the medium plot. The bias of the extracted stem curves was 0.3 cm (1.2%) in the easy plot and 0.5 cm (2.1%) in the medium plot. These results are illustrated in Fig. 9(a). In Fig. 9(b), we provide a scatter plot of the stem curve estimates against the reference measurements. The coefficient of determination R^2 was 0.90 for the easy plot and 0.95 for the medium plot.

Note that the trees in the easy plot are fairly homogeneous with only small variations in the diameter estimates, which explains the fact that

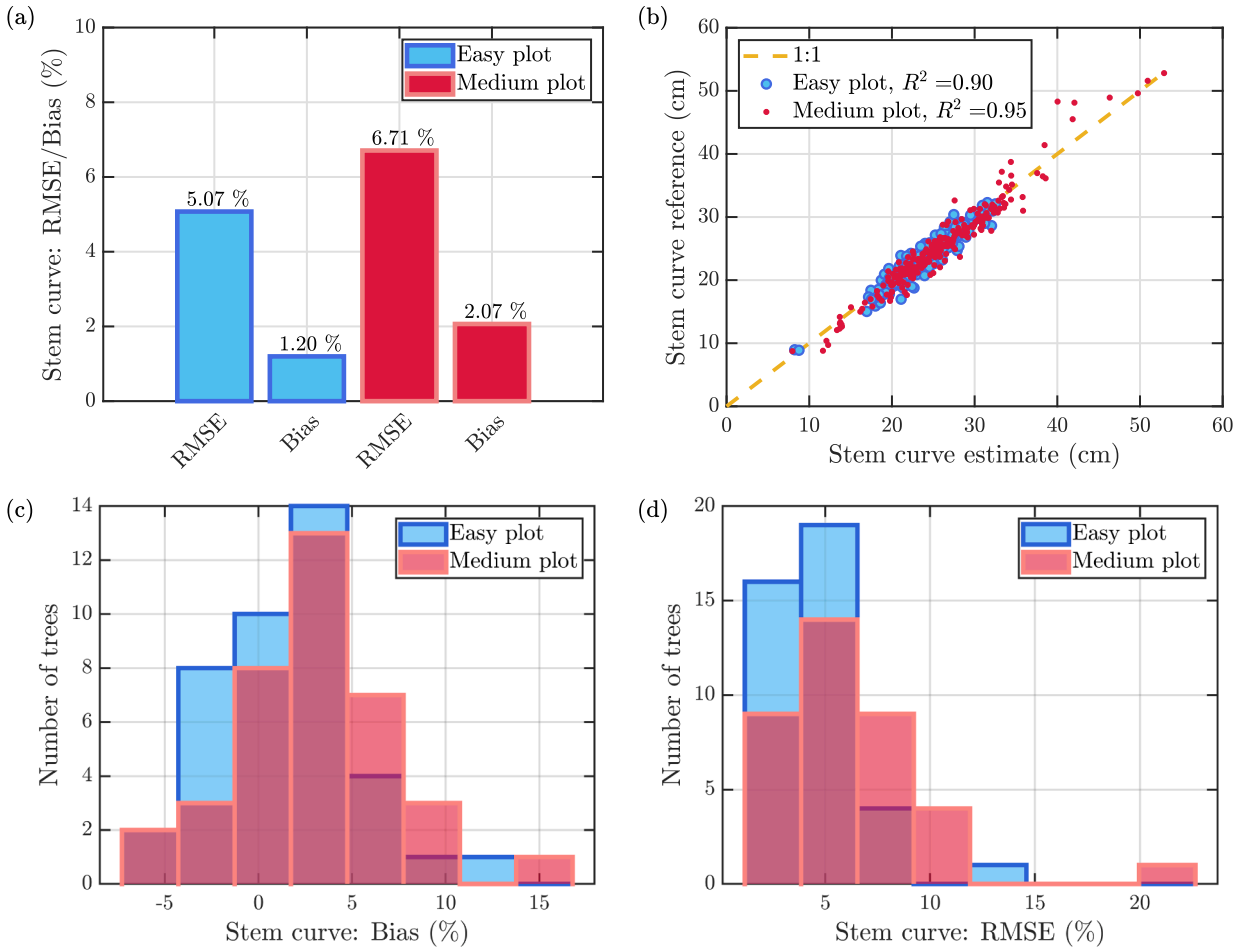

Fig. 9. (a) Relative RMSE and bias of the stem curve estimates at the individual tree level for the easy plot (blue) and for the medium plot (red). (b) Scatter plot of the stem curve estimates vs the reference stem curve values in the easy (blue circles) and medium plots (red circles). The scatter plot shows the diameter estimates of all the matched trees at such heights for which both the estimated and the reference diameter are available. The coefficient of determination is R^2 = 0.90 for the easy plot and R^2 = 0.95 for the medium plot. (c) Histogram of the relative biases of the stem curves at the individual tree level for the easy plot (blue) and for the medium plot (red). (d) Histogram of the relative RMSE values of the stem curves at the individual tree level for the easy plot (blue) and for the medium plot (red).

the coefficient of determination is lower in the easy plot despite of the better relative accuracy. Fig. 9(c) and (d) illustrate the relative bias and RMSE values of the stem curves for individual stems. Of note, the RMSE is less than 15% for all trees except for one small birch, whereas previous MLS studies on similar test sites have reported mean relative RMSE values that are greater than 15% for easy plots (Liang et al., 2018b).

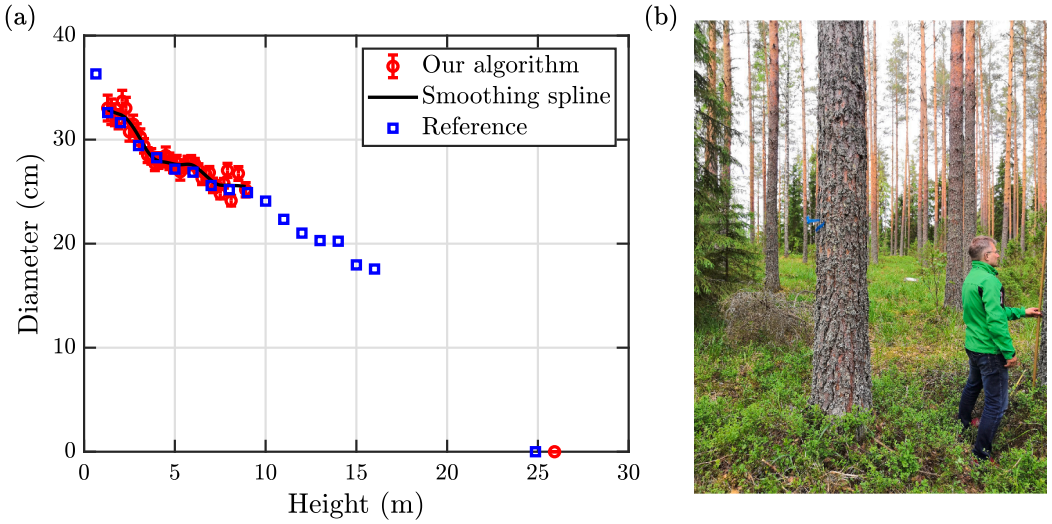

Fig. 10. (a) Example stem curve of a pine in the medium plot. The red circles depict the diameter estimates extracted using our algorithm, whereas the corresponding reference measurements are denoted with blue squares. The error bars show the standard deviation of the radial residuals after the arc matching algorithm. The smoothing spline fit to the extracted stem curve is illustrated with the solid black line. For this pine, the bias of the diameter estimates is 0.47 cm = 1.7% and the corresponding RMSE value is 0.57 cm = 2.0%. (b) Photograph of the pine whose stem curve is visualized in the panel (a).

In Fig. 10, we show an example of a stem curve extracted using our algorithm together with a photograph of the corresponding tree in order to illustrate the performance of the proposed method. The figure presents a typical stem curve of a pine whose stem is not occluded by any smaller trees. As can be seen from the figure, the stem curve can be extracted with high precision almost up to the height of 10 m. The high accuracy of the stem curve extraction is a result of the fairly circular cross section of the tree and a low number of branches in the lower part of the stem.

4.3. Tree height

The bias of tree height estimation (as described in Section 3.5) was 1.3 m (6.0%) in the easy plot and 0.68 m (3.0%) in the medium plot. The corresponding RMSE values are 1.8 m (8.7%) and 1.1 m (4.9%) for the easy and medium plot, respectively. The positive bias of the height estimation implies that the heights determined from the MLS point cloud are overestimated as compared with the reference ALS measurements. There are a few possible reasons for this slightly counter-intuitive result. First, both of the plots contain a single small tree whose height was overestimated by roughly 5 m since the tree top of the small tree is located inside the canopy of one of its neighboring trees. For example, this occurs for the small birch illustrated in Fig. A16. Second, the error in the tree height seems to depend systematically on the tree location in the easy plot. This is most likely an artefact resulting from the SLAM algorithm. Third, the MLS point cloud has a significantly higher point density than the corresponding ALS point cloud and therefore, it is probable that some of the tree tops are actually more accurately captured by the MLS point cloud.

4.4. Stem volume

In order to assess the performance of our method for volume estimation, we estimate both the volume of the whole stem and the stem volume in the interpolation range. The 'interpolation range' is the height interval for which both the reference measurements and the estimated diameters are available. Fig. 11(a) illustrates the process of determining the volume of the whole stem for an example tree. Note that even in an optimal case, we manage to extract the stem curve reliably only up to the height of 10 m, and therefore we need to use a model with few parameters when extrapolating the stem curve in order to avoid artefacts caused by overfitting.

In the interpolation range, the bias of the estimated volume was 1.6% for the easy plot and 3.0% for the medium plot. The corresponding RMSE values were 6.6% for the easy plot and 11.6% for the medium plot. We have estimated that the interpolation range contains on average 47% of the volume of the entire stem in the easy plot and 46% of the volume of the entire stem in the medium plot.

Subsequently, we consider the accuracy of estimating the volume of the entire stem with the proposed method. The stem volume estimates are visualized in 11(b) using a scatter plot. In the easy plot, the bias of the volume estimates was 0.012 m^3 (2.2%), whereas the corresponding RMSE error was 0.053 m^3 (9.7%). In the medium plot, the bias of the volume estimates was − 0.002 m^3(−0.3 %), and the RMSE error was 0.083 m^3 (10.9%). The average stem volume based on the reference measurements was 0.54 m^3 in the easy plot, and 0.76 m^3 in the medium plot.

To demonstrate the performance of the proposed method, we further compare our results against volume estimates computed using the Finnish allometric model established by Laasasenaho (1982) as illustrated in Fig. 11(c) and (d). In applying the allometric model, we used field measured DBH and tree height as inputs and took into account the species of the tree, and compared the resulting estimates to the reference data. In the easy plot, the bias of the resulting volume estimates was − 1.5% and the corresponding relative RMSE error equaled 11.7%. In the medium plot, the bias of the allometrically predicted volumes was − 3.8%, whereas the relative RMSE was as large as 26.0%. The large RMSE of the allometrically predicted volumes in the medium plot is mainly due to one large birch whose volume (V_{ref} = 3.0 m^3) is severely underestimated ($V_{allometric}$ = 1.9 m^3) by the allometric model. If the large birch is neglected from the analysis, we obtain approximately 10% for the relative RMSE of the stem volumes predicted by the allometric model. Thus, the accuracy of our method presented herein was equivalent or better than that of the allometric model for the two test sites.

5. Discussion

5.1. Comparison with past studies

Tree detection - Many previous works have been carried out in the pursuit of tree detection. Bauwens et al. (2016) detected 91% of the trees using handheld MLS. In a study conducted by Bienert et al. (2018), 87.5% of trees were detected in the leaf- off dataset with eight commission errors in one plot and 100% of trees with 49 commission errors in the other plot. In Zhao et al. (2018), HiScan-Z mobile laser scanning system resulted in correctness and completeness rates of better than 92% for street trees. Wu et al. (2013) applied MLS System of East China Normal University and concluded that street tree detection is over 98%. Liang et al. (2018b, 2019) reported tree detection rate of 95% in easy and 82% in medium forests. Thus, our algorithm enables tree detection with completeness and correctness levels on par with other state-of-the-art approaches since we achieve a completeness rate of 95% in the easy plot and 84% in the medium plot, and the correctness level is 100% for both the plots.

Diameter at breast height and stem curve - The international benchmarking with TLS data showed that multi-scan TLS allows for DBH estimation with a relative RMSE of 5–10% in easy and medium visibility forest stands (Liang et al., 2018a). Phone-based mobile laser scanning (SLAM included) has been studied by Fan et al. (2018), Hyyppä et al. (2017), Tomaštik et al. (2017) using Google Tango. Tomaštik et al. (2017) included approximately 120 trees using CloudCompare software in which the DBHs were manually measured using a point-to- point measurement tool, and the RMSE of DBHs was approximately 2 cm. Hyyppä et al. (2017) used automated circle fitting to estimate the DBH and found that the obtained results matched those from tape measurements with an RMSE of 0.73 cm. In Fan et al. (2018), the Levenberg-Marquardt algorithm was used in the analysis of the point clouds resulting in an RMSE of 1.26 cm (6.39%) for DBH. In an attempt to measure several dozens of plots in a day, the phone-based approach is much too time-consuming since it requires measuring every tree separately (Hyyppä et al., 2017). In previous hand-held scanner studies, represented by various Zebedee solutions and commercial high-end SLAM solutions, the reported accuracy of DBH estimation ranges from about 1 cm in easy urban forests (Cabo et al., 2018; Bauwens et al., 2016; Del Perugia et al., 2019) to 2.5–4 cm depending on the forest type (Marselis et al., 2016; Del Perugia et al., 2019).

There are only a few papers reporting the accuracy of stem curve estimation. In Liang et al. (2018b), the relative RMSE of TLS-based stem curve estimation was found to be less than 10% in various forests. The corresponding RMSE values based on MLS data were 18% and 30% for easy and medium difficult forests, respectively. They concluded that as the forest complexity increased, the quality of the point cloud data decreased due to the reduced positioning accuracy, the decreased accessibility of the plot and the coverage of data, and the increased occlusion effects. Due to these problems, MLS-based stem curve extraction has not before been accurate enough for deriving the stem volume with a low RMSE. In our study, these problems are greatly alleviated by the improved data processing work flow allowing for accurate MLS-based stem curve modeling. As a result, the accuracy of stem curve extraction using our method is on par with the previously reported results obtained with TLS in similar forest stand conditions (Liang et al., 2018b and Liang et al., 2018a).

Tree Height – Several previous studies have highlighted the low quality of tree height estimates derived from MLS data. For example,

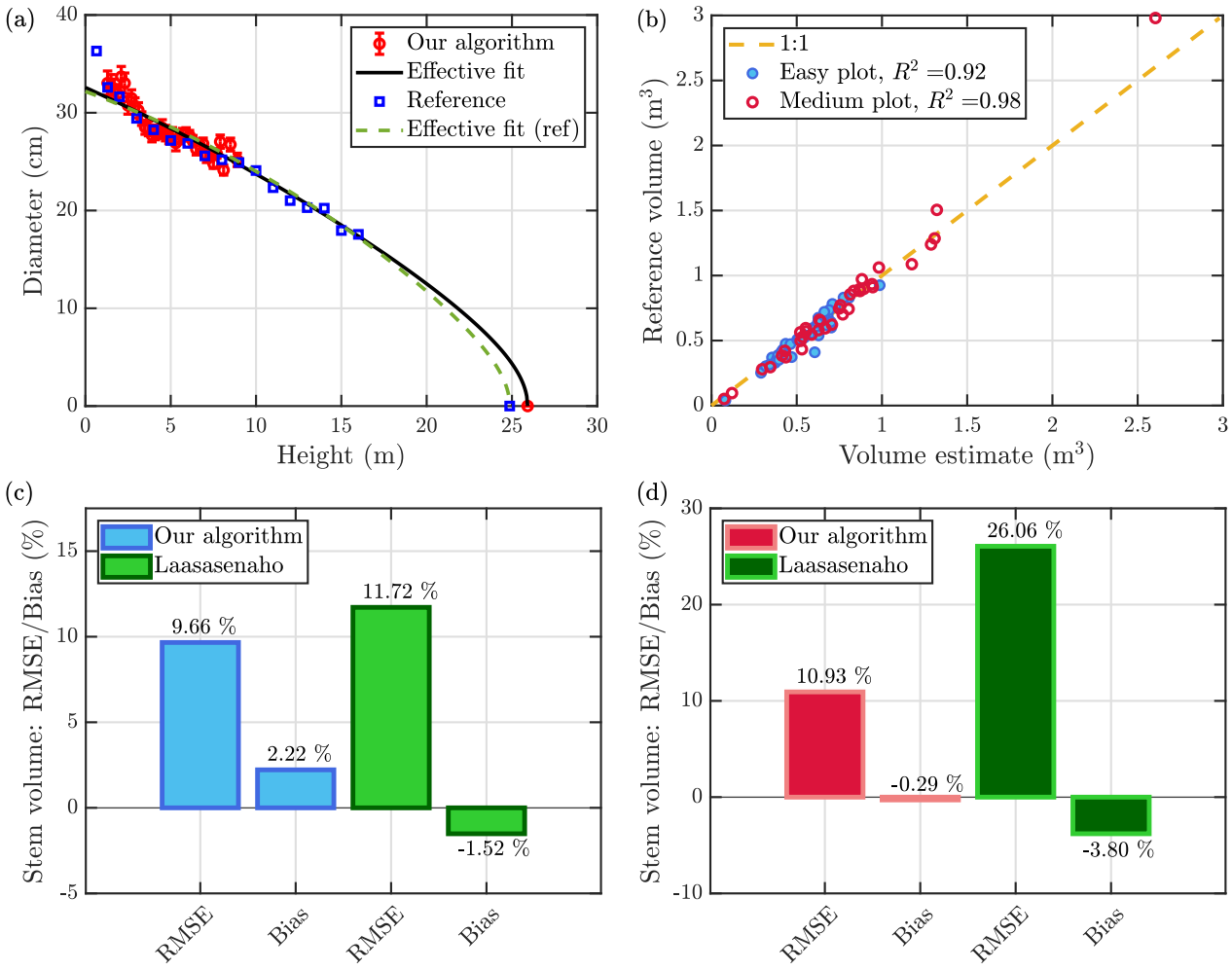

Fig. 11. (a) Estimated stem curve of an example pine (red circles) with the effective fit (solid black line) based on Eqs. (1) and (2). The effective fit is used to extrapolate the volume of the whole tree. Furthermore, we show the reference diameter values (blue squares) with the corresponding effective fit (dashed green line) used to estimate the reference volume of the whole tree. (b) Extrapolated stem volume vs the reference stem volume for the easy (blue circles) and medium plots (red circles). The coefficient of determination is $R^2 = 0.92$ for the easy plot, and $R^2 = 0.98$ for the medium plot. (c) Relative RMSE and bias for the volume estimates of the whole stem in the easy plot. The blue bars show the results of our algorithm, whereas the green bars depict the results obtained by applying the allometric Laasasenaho model to field measurements. (d) Same as panel (c) but for the medium plot.

Liang et al. (2019) reported 10% underestimation and more than 30% standard deviation for tree height estimation in medium difficult boreal forests using phase-shift ranging laser. The major added value of the approach used here is that the applied backpack laser scanner is pulse-based allowing several returns per pulse to be recorded from longer distances. The data also provided good ground reference for the height determination.

Stem Volume – we note that our method allows one to extract the stem volumes with an accuracy that is by far better than the results reported previously using MLS data (from 20 to 50% error for easy and medium easy plots) obtained with MLS (Liang et al., 2018b, 2019; Bienert et al., 2018) and on par with the accuracy of stem volume estimation using TLS in similar forest conditions (Liang et al., 2018b). Recently, Liang et al. (2019) evaluated the performance of UAV LS for 22 sample plots of various forest stand conditions in a boreal forest: the tree attributes were compared with state-of-the-art terrestrial and mobile laser scanning and the results showed that in easy forest stand conditions, the performance of UAV LS point cloud is comparable with the terrestrial solutions with relative RMSE less than 20% for stem diameter and 50% for stem volume. Some have suggested that the combination of UAV LS and TLS is the first solution to reach accuracies required for field inventory reference data (e.g. 10%). Herein, we have demonstrated that our approach using MLS data can achieve the desired level of accuracy.

5.2. Applicability and further developments

As illustrated in Fig. 12, the workflow proposed in this paper allows us to extract the stem curve accurately from a wide height interval. The RMSE of stem curves is below 6% all the way up to the height of 8 m in the easy plot, and the RMSE stays below 9% at all heights up to 9 m in the case of the medium plot. Interestingly, the RMSE is the smallest at the height of 4 m for both of the plots. At the height of 4 m, the RMSE is approximately 4% for both of the plots. The bias of the stem curve estimates shows a slightly declining trend in the height range 1–8 m. Note that the RMSE and bias values corresponding to the height of 9 m are based on a small number of trees since there are only 3 (7) trees in the easy (medium) plot, for which we can obtain the stem diameter estimate at this height.

It is natural that the RMSE increases high above the ground for a couple of reasons: first, the number of branches increases as we approach the top of the tree. Second, the distance from the scanner to the stem increases the higher we go, which results in a decreased measurement accuracy and an increased spacing between consecutive points. Both of these effects result in a smaller number of good quality arcs.

In terms of sampling effort, MLS is an effective and efficient data collection tool. Based on our tests in Finnish boreal forests, it is possible

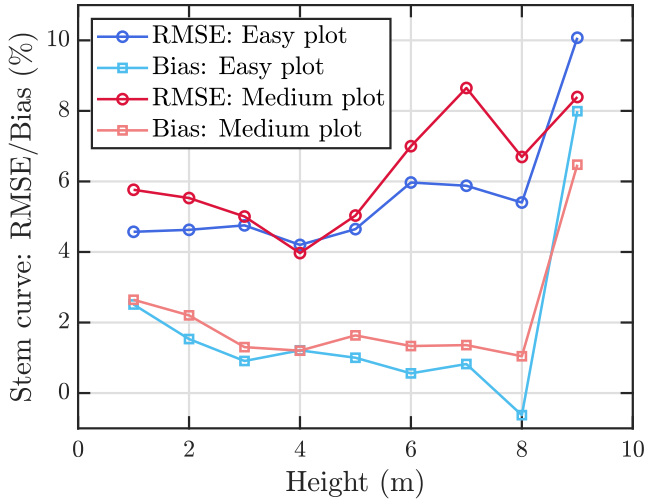

Fig. 12. RMSE and bias of stem curve in the easy and medium plots as a function of height from ground. Note that a positive bias indicates that our estimates for stem diameter are on average larger than the corresponding reference values. To evaluate the bias and RMSE at a given height, we only consider such trees, for which the stem diameter estimate exists at the given height.

Fig. 13. An example of a spruce in the medium plot whose stem could not be detected by the arc-based algorithm due to the high density of branches causing laser beam occlusion of the stem.

for a single surveyor to collect data from approximately 40 forest plots in a single day. In contrast, a team of two surveyors applying conventional measurement methods can only measure two sample plots in a single day. If the multi-scan technique is applied, TLS measurements can be conducted for half a dozen sample plots in a single day. One potential solution to improve the data collection efficiency of MLS even further is to use stripwise plots. In this approach that we are currently studying, the data is collected along an approximately linear working path of the surveyor and the same path may be recollected to get loop closure for SLAM processing. Such a concept would provide more reference data in a more cost-effective way.

Importantly, the algorithm for MLS data processing presented herein is feasible from the point of view of the computation time. Using our Matlab implementation, we can process a single point cloud containing 215 million points (~5 GB in las-format) in approximately 30 min on a modern laptop computer. The two point clouds studied in this work cover an area of approximately 0.2 ha each. This implies that during a single day, our implementation of the algorithm could process a point cloud covering 10 ha assuming that the point density is as high as 1.1×10^5 pts/m^2. Note that this means that both the data acquisition and the data processing are capable of reaching the > 40 sample plots/day limit. With further parallelization and optimization, the running time of the proposed algorithm can potentially be greatly reduced.

In this paper, the focus was on finding and measuring the trees with visible stems. In Finnish boreal forests, this means pines and birches. The approach possibly works for other broad-leaved species such as oak, maple, aspen, mountain ash, linden and alder.

One important research step for the future is to improve the capability of the proposed method in more complex forests. Spruce is also a very common tree species in Finland and would need to be measured and modelled with different approaches due to the occlusion of the stem arising from the high number of branches. Fig. 13 illustrates the occlusion problem by showing a photograph of a spruce whose stem could not be detected. Old spruces have visible trunks and similar algorithms as presented in this study can be applied. Youngest spruces should be measured using their outer shape and stem properties should be estimated from their height and crown diameters at each height. Those in between should apply approaches that find the trunks from very noisy data. Solutions based on surface normal may help. Additionally, one should note that complex forests provide challenges for SLAM and georeferencing of the data prior processing. Multibeam laser scanning may provide a SLAM solution in complex forests.

There are areas where individual tree based forest inventory could be needed, but it is not currently applied due to the lack of field reference data at individual tree level. Techniques in this paper allow for the collection of field data cost-effectively. Individual tree -based inventory will lead to increased accuracy of forest data, which can lead to increase in the society savings.

6. Conclusions

In the scientific literature, the combination of TLS and UAV LS is often purported as the required future solution to estimating individual tree stem volumes with sufficient accuracy for operational applications (i.e. relative RMSE of approximately 10%). Herein, we tested an approach based on a pulse-based backpack laser scanner for estimating stem volumes in Finnish boreal forest conditions. We applied in-house developed SLAM and novel algorithms using post-SLAM and inclination angle correction to derive stem curves of the standing trees from high-quality arcs. By using the derived stem curves and tree heights, stem volume estimates for trees in easy and medium boreal forest plots were calculated. We note that our approach and processing method allows one to extract stem volumes for pines and birches with an accuracy that clearly exceeds the previously reported values obtained using MLS data. Importantly, the RMSE of stem volume estimation (~10%) is on par with methods using data integrated from multiscan TLS and tree height measurements. In addition, we were able to measure tree heights with the accuracy required for operational forest inventories. Since the bias of the method was small, our approach can also be used to provide plot level estimates. Therefore, the findings are important steps towards future individual-tree-based ALS inventories.

Acknowledgements

Academy of Finland is gratefully acknowledged for funding this study mainly through the project Centre of Excellence in Laser Scanning Research (CoE-LaSR) (307362)“ and partially through Strategic Research Council at the Academy of Finland project Competence-Based Growth Through Integrated Disruptive Technologies of 3D Digitalization, Robotics, Geospatial Information and Image Processing/Computing “ Point Cloud Ecosystem (293389 / 314312).

Author contributions

The paper can be considered as joint first authorship with E.H. and A.K. J.H. acted as senior author and supervisor in all steps. E.H. developed the processing methods based on ideas and experimental plan provided by J.H. and A.K. E.H. implemented all algorithms, processed data, results and wrote most of the article getting contributions from J.H. and A.K. M.W. and J.W. provided insights through out the paper and improved the manuscript. E.H. and J.H. collected field data in 2019 needed for growth compensation. A.K. developed the AkhkaR3 MLS hardware, collected and pre-processed the data. He also initiated and led the development of the graph SLAM algorithm, implemented by R.K. J.P. processed the field reference stem curves. X.Y. provided basic algorithms and other field reference for E.H. to initialize the work. X.L., J-P.V., Y.W, X.Y., and H.K. participated in improving the manuscript.

Appendix

In this section, we show a few more examples of the stem curves that were extracted using our algorithm. Fig. A.14 shows the stem diameter as a function of height for a pine whose stem curve is accurately extracted by our algorithm thanks to a fairly circular stem section and minimal occlusion of the stem.

Importantly, the proposed workflow succeeds in extracting the stem curve also for more difficult trees. Figs. A.15–A.17 illustrate stem curves of trees that are much more challenging due to a variety of reasons. Fig. A.15(a) shows the stem curve of a pine whose trunk is partly occluded by the branches of a nearby spruce. As can be seen from Fig. A15, the algorithm can still find arcs of good quality from that side of the pine trunk that is not surrounded by the branches of the spruce. Additionally, our arc-based method naturally filters out data points corresponding to the branches of the spruce before the circle fitting process.

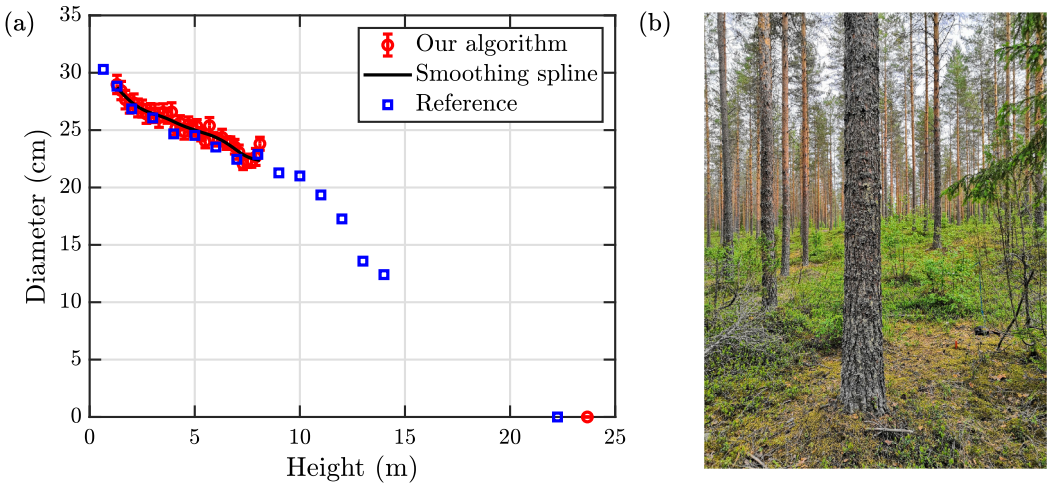

Fig. A14. (a) Stem curve of a pine in the easy plot. The red circles depict the diameter estimates extracted using our algorithm, whereas the corresponding reference measurements are denoted with blue squares. The error bars show the standard deviation of the radial residuals after the arc matching algorithm. The smoothing spline fit to the extracted stem curve is illustrated with the solid black line. For this pine, the bias of the diameter estimates is 0.44 cm = 1.8% and the corresponding RMSE value is 0.65 cm = 2.6%. (b) Photograph of the pine whose stem curve is visualized in the panel (a).

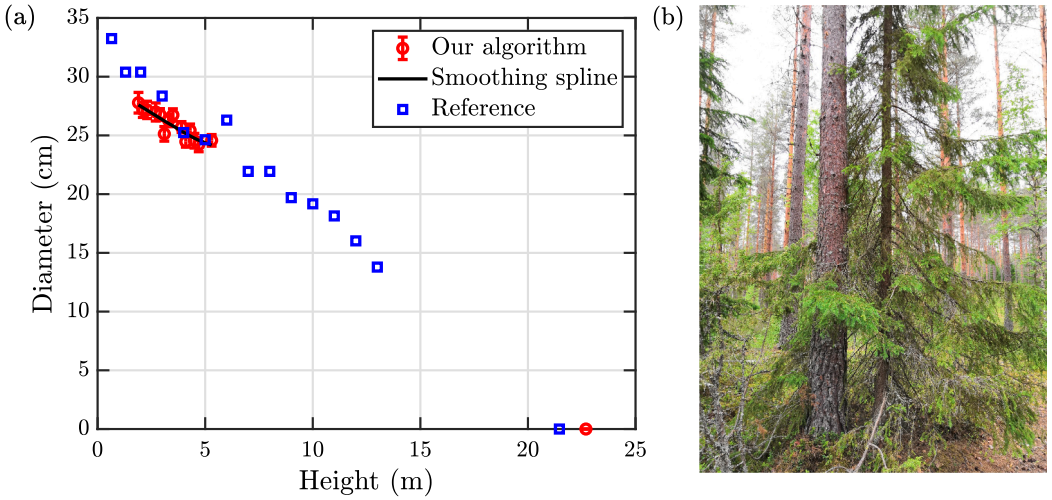

Fig. A15. (a) Stem curve of a pine that is located next to a smaller spruce whose branches surround the stem of the pine at some heights. The red circles depict the diameter estimates extracted using our algorithm, whereas the corresponding reference measurements are denoted with blue squares. The error bars show the standard deviation of the radial residuals after the arc matching algorithm. The smoothing spline fit to the extracted stem curve is illustrated with the solid black line. For this pine, the bias of the diameter estimates is −1.3 cm = -4.7% and the corresponding RMSE value is 1.9 cm = 6.5%. (b) Photograph of the pine whose stem curve is visualized in the panel (a). Note the spruce on the right of the pine.

In Fig. A16(a), we show the stem curves of two birches that are located right next to each other as illustrated in Fig. A16(b). Since the positioning error of individual points is on the order of 10–20 cm after the SLAM algorithm, it is possible to resolve the birches from one another in the clustering step of the algorithm (see Sec. 3.2). Due to the large inclination angle of the smaller birch ($\theta = 8.6°$), the PCA correction described in Sec. 3.3 is vital in obtaining an accurate estimate of the stem curve. The fairly large RMSE error in the stem curve of the larger birch (2.6 cm = 10.4%) can be attributed to its fairly non-circular stem.

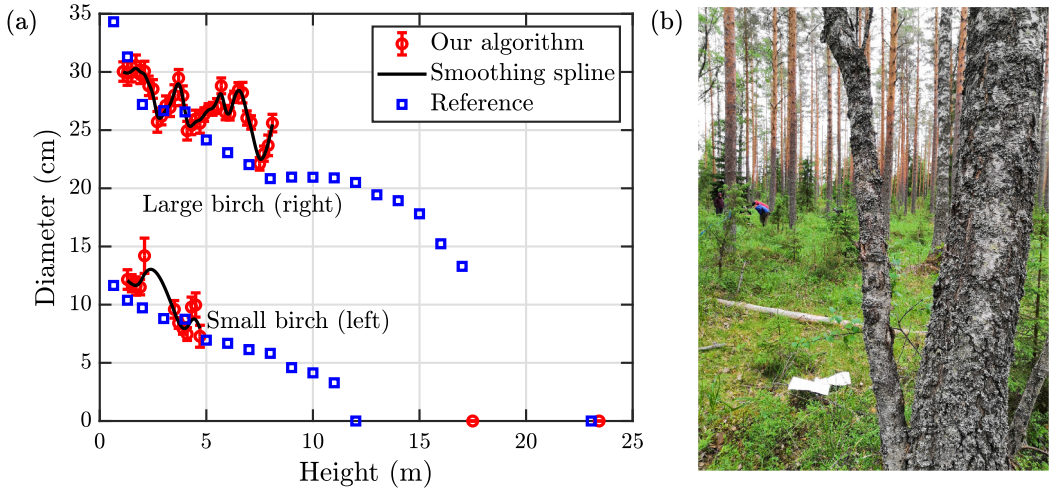

Fig. A16. (a) Stem curves of two birches that are located right next to each other. The red circles depict the diameter estimates extracted using our algorithm, whereas the corresponding reference measurements are denoted with blue squares. The error bars show the standard deviation of the radial residuals after the arc matching algorithm. The smoothing spline fit to the stem curve is illustrated with the solid black line. Note that our algorithm overestimates the height of the smaller birch by roughly 5 m even though the algorithm recognizes it as a suppressed tree. This is due to the fact that the tree top of the smaller birch is practically located within the crown of the larger birch. For the larger birch, the bias of the diameter estimates is 1.8 cm = 7.2% and the corresponding RMSE value is 2.6 cm = 10.4%, whereas the corresponding values for the smaller birch are bias = 1.6 cm = 16.8% and RMSE = 2.1 cm = 22.6%. (b) Photograph of the birches whose stem curves are visualized in the panel (a). The large birch is shown on the right in the image, whereas the smaller birch is located on its left side.

Fig. A17(a) illustrates the stem curve of the only spruce detected with our algorithm in the medium plot. As shown in Fig. A17(b), the branches located in the lower part of the spruce have dropped a significant proportion of their needles. Due to the moderate visibility of the stem, it is possible to obtain arcs of good quality from a reasonably wide height interval since our arc extraction algorithm can handle noise points in the middle of an arc as explained in Sec. 3.2. Note also that the existence of outlying diameter estimates (see definition in Sec. 3.4) is rare even for difficult trees.

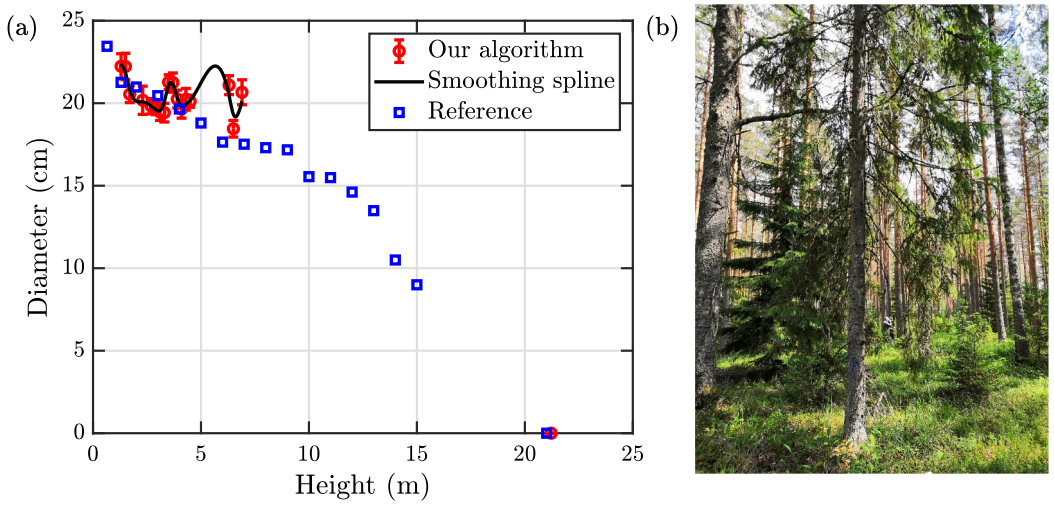

Fig. A17. (a) Stem curve of a spruce that has dropped its lowest branches. The red circles depict the diameter estimates extracted using our algorithm, whereas the corresponding reference measurements are denoted with blue squares. The error bars show the standard deviation of the radial residuals after the arc matching algorithm. The smoothing spline fit to the extracted stem curve is illustrated with the solid black line. For this spruce, the bias of the stem curve estimates is 1.05 cm = 5.3%, whereas the corresponding RMSE value is 2.1 cm = 10.6%. (b) Photograph of the spruce whose stem curve is visualized in the panel (a).

References

Al-Sharadqah, A., Chernov, N., 2009. Error analysis for circle fitting algorithms. Electron. J. Statist. 3, 886–911.

Bauwens, S., Bartholomeus, H., Calders, K., Lejeune, P., 2016. Forest invent tory with terrestrial lidar: a comparison of static and hand-held mobile laser scanning. Forests 7, 127.

Bienert, A., Georgi, L., Kunz, M., Maas, H.G., von Oheimb, G., 2018. Comparison and combination of mobile and terrestrial laser scanning for natural forest inventories. Forests 9, 395.

Cabo, C., Del Pozo, S., Rodríguez-Gonzálvez, P., Ordóñez, C., González-Aguilera, D., 2018. Comparing terrestrial laser scanning (tls) and wearable laser scanning (wls) for individual tree modeling at plot level. Remote Sens. 10, 540.
Čerňava, J., Mokroš, M., Tuček, J., Antal, M., Slatkovská, Z., 2019. Processing chain for estimation of tree diameter from gnss-imu-based mobile laser scanning data. Remote Sens. 11, 615.
Chen, S., Liu, H., Feng, Z., Shen, C., Chen, P., 2019. Applicability of personal laser scanning in forestry inventory. PLoS ONE 14, e0211392.
De Boor, C., 1978. A practical guide to splines. volume 27. springer-verlag, New York.
Del Perugia, B., Giannetti, F., Chirici, G., Travaglini, D., 2019. Influence of scan density on the estimation of single-tree attributes by hand-held mobile laser scanning. Forests 10, 277.
Ester, M., Kriegel, H.P., Sander, J., Xu, X., 1996. A density-based algorithm for discovering clusters in large spatial databases with noise. In: Kdd, pp. 226–231.
Fan, Y., Feng, Z., Mannan, A., Khan, T., Shen, C., Saeed, S., 2018. Estimating tree position, diameter at breast height, and tree height in real-time using a mobile phone with rgb-d slam. Remote Sens. 10, 1845.
Forsman, M., Börlin, N., Olofsson, K., Reese, H., Holmgren, J., 2018. Bias of cylinder diameter estimation from ground-based laser scanners with different beam widths: a simulation study. ISPRS J. Photogramm. Remote Sens. 135, 84–92.
Forsman, M., Holmgren, J., Olofsson, K., 2016. Tree stem diameter estimation from mobile laser scanning using line-wise intensity-based clustering. Forests 7, 206.
Haara, A., Kangas, A., Tuominen, S., 2019. Economic losses caused by tree species proportions and site type errors in forest management planning.
Holmgren, J., Tulldahl, M., Nordlöf, J., Willén, E., Olsson, H., 2019. Mobile laser scanning for estimating tree stem diameter using segmentation and tree spine calibration. Remote Sens. 11, 2781.
Hyyppä, J., Kelle, O., Lehikoinen, M., Inkinen, M., 2001. A segmentation based method to retrieve stem volume estimates from 3-d tree height models produced by laser scanners. IEEE Trans. Geosci. Remote Sens. 39, 969–975.
Hyyppä, J., Virtanen, J.P., Jaakkola, A., Yu, X., Hyyppä, H., Liang, X., 2017. Feasibility of google tango and kinect for crowdsourcing forestry information. Forests 9, 6.
Junttila, S., Vastaranta, M., Liang, X., Kaartinen, H., Kukko, A., Kaasalainen, S., Holopainen, M., Hyyppä, H., Hyyppä, J., 2017. Measuring leaf water content with dual-wavelength intensity data from terrestrial laser scanners. Remote Sens. 9, 8.
Kaartinen, H., Hyyppä, J., Vastaranta, M., Kukko, A., Jaakkola, A., Yu, X., Pyörälä, J., Liang, X., Liu, J., Wang, Y., et al., 2015. Accuracy of kinematic positioning using global satellite navigation systems under forest canopies. Forests 6, 3218–3236.
Kangas, A., Haara, A., Holopainen, M., Luoma, V., Packalen, P., Packalen, T., Ruotsalainen, R., Saarinen, N., 2019. Kaukokartoitukseen perustuvan metsävaratiedon hyötyanalyysi: Metku-hankkeen loppuraportti.
Kåsa, I., 1976. A circle fitting procedure and its error analysis. IEEE Trans. Instrum. Meas. 8–14.
Kettunen, M., Vihervaara, P., Kinnunen, S., D'Amato, D., Badura, T., Argimon, M., Ten Brink, P., 2012. Socio-economic importance of ecosystem services in the Nordic Countries – Synthesis in the context of The Economics of Ecosystems and Biodiversity (TEEB). Nordic Council of Ministers.
Koskela, L., Nummi, T., Wenzel, S., Kivinen, V.P., 2006. On the analysis of cubic smoothing spline-based stem curve prediction for forest harvesters. Can. J. For. Res. 36, 2909–2919.
Kukko, A., Kaijaluoto, R., Kaartinen, H., Lehtola, V.V., Jaakkola, A., Hyyppä, J., 2017. Graph slam correction for single scanner mls forest data under boreal forest canopy. ISPRS J. Photogramm. Remote Sens. 132, 199–209.
Laasasenaho, J., 1982. Taper curve and volume functions for pine, spruce and birch. Metsäntutkimuslaitos.
Liang, X., Hyyppä, J., Kaartinen, H., Lehtomäki, M., Pyörälä, J., Pfeifer, N., Holopainen, M., Brolly, G., Francesco, P., Hackenberg, J., et al., 2018a. International benchmarking of terrestrial laser scanning approaches for forest inventories. ISPRS J. Photogramm. Remote Sens. 144, 137–179.
Liang, X., Kankare, V., Yu, X., Hyyppä, J., Holopainen, M., 2014a. Automated stem curve measurement using terrestrial laser scanning. IEEE Trans. Geosci. Remote Sens. 52, 1739–1748.
Liang, X., Kukko, A., Hyyppä, J., Lehtomäki, M., Pyörälä, J., Yu, X., Kaartinen, H., Jaakkola, A., Wang, Y., 2018b. In-situ measurements from mobile platforms: An emerging approach to address the old challenges associated with forest inventories. ISPRS J. Photogramm. Remote Sens. 143, 97–107.
Liang, X., Kukko, A., Kaartinen, H., Hyyppä, J., Yu, X., Jaakkola, A., Wang, Y., 2014b. Possibilities of a personal laser scanning system for forest mapping and ecosystem services. Sensors 14, 1228–1248.
Liang, X., Litkey, P., Hyyppa, J., Kaartinen, H., Vastaranta, M., Holopainen, M., 2012. Automatic stem mapping using single-scan terrestrial laser scanning. IEEE Trans. Geosci. Remote Sens. 50, 661–670.
Liang, X., Wang, Y., Pyörälä, J., Lehtomäki, M., Yu, X., Kaartinen, H., Kukko, A., Honkavaara, E., Issaoui, A.E., Nevalainen, O., et al., 2019. Forest in situ observations using unmanned aerial vehicle as an alternative of terrestrial measurements. Forest Ecosystems 6, 20.
Lovell, J., Jupp, D.L., Culvenor, D., Coops, N., 2003. Using airborne and ground-based ranging lidar to measure canopy structure in australian forests. Can. J. Remote Sens. 29, 607–622.
Marselis, S.M., Yebra, M., Jovanovic, T., van Dijk, A.I., 2016. Deriving comprehensive forest structure information from mobile laser scanning observations using automated point cloud classification. Environ. Modell. Software 82, 142–151.
Nummi, T., Möttönen, J., 2004. Prediction of stem measurements of scots pine. J. Appl. Stat. 31, 105–114.
Pierzchała, M., Giguère, P., Astrup, R., 2018. Mapping forests using an unmanned ground vehicle with 3d lidar and graph-slam. Comput. Electron. Agric. 145, 217–225.
Pollock, D., 1993. Smoothing with cubic splines.
Pratt, V., 1987. Direct least-squares fitting of algebraic surfaces. In: ACM SIGGRAPH computer graphics, ACM. pp. 145–152.
Raumonen, P., Kaasalainen, M., Åkerblom, M., Kaasalainen, S., Kaartinen, H., Vastaranta, M., Holopainen, M., Disney, M., Lewis, P., 2013. Fast automatic precision tree models from terrestrial laser scanner data. Remote Sens. 5, 491–520.
Saarela, S., Breidenbach, J., Raumonen, P., Grafström, A., Ståhl, G., Ducey, M.J., Astrup, R., 2017. Kriging prediction of stand-level forest information using mobile laser scanning data adjusted for nondetection. Can. J. For. Res. 47, 1257–1265.
Saarinen, N., Kankare, V., Vastaranta, M., Luoma, V., Pyörälä, J., Tanhuanpää, T., Liang, X., Kaartinen, H., Kukko, A., Jaakkola, A., et al., 2017. Feasibility of terrestrial laser scanning for collecting stem volume information from single trees. ISPRS J. Photogramm. Remote Sens. 123, 140–158.
Tomaštik, J., Salon, Š., Tunák, D., Chud, F., Kardoš, M., 2017. Tango in forests – an initial experience of the use of the new google technology in connection with forest inventory tasks. Comput. Electron. Agric. 141, 109–117.
Wang, Y., Lehtomäki, M., Liang, X., Pyörälä, J., Kukko, A., Jaakkola, A., Liu, J., Feng, Z., Chen, R., Hyyppä, J., 2019a. Is field-measured tree height as reliable as believed – a comparison study of tree height estimates from field measurement, airborne laser scanning and terrestrial laser scanning in a boreal forest. ISPRS J. Photogr. Remote Sens. 147, 132–145.
Wang, Y., Pyörälä, J., Liang, X., Lehtomäki, M., Kukko, A., Yu, X., Kaartinen, H., Hyyppä, J., 2019b. In situ biomass estimation at tree and plot levels: What did data record and what did algorithms derive from terrestrial and aerial point clouds in boreal forest. Remote Sens. Environ. 232, 111309.
Wu, B., Yu, B., Yue, W., Shu, S., Tan, W., Hu, C., Huang, Y., Wu, J., Liu, H., 2013. A voxel-based method for automated identification and morphological parameters estimation of individual street trees from mobile laser scanning data. Remote Sensing 5, 584–611.
Zhao, Y., Hu, Q., Li, H., Wang, S., Ai, M., 2018. Evaluating carbon sequestration and pm2. 5 removal of urban street trees using mobile laser scanning data. Remote Sens. 10, 1759.
Zianis, D., Muukkonen, P., Mäkipää, R., Mencuccini, M., 2005. Biomass and stem volume equations for tree species in Europe. Silva Fennica Monographs 4, 1–63.